JOURNAL OF GEOPHYSICAL RESEARCH, VOL. 101, NO. D5, PAGES 9441-9470, APRIL 27, 1996

Stratospheric horizontal wavenumber spectra of winds, potential temperature, and atmospheric tracers observed by high-altitude aircraft

Julio T. Bacmeister,[1] Stephen D. Eckermann,[2] Paul A. Newman,[3] Leslie Lait,[3]
K. Roland Chan,[4] Max Loewenstein,[4] Michael H. Proffitt,[5] Bruce L. Gary[6]

Abstract. Horizontal wavenumber power spectra of vertical and horizontal wind velocities, potential temperatures, and ozone and N_2O mixing ratios, as measured in the mid-stratosphere during 73 ER-2 flights (altitude $\approx$ 20km) are presented. The velocity and potential temperature spectra in the 100 to 1-km wavelength range deviate significantly from the uniform $-5/3$ power law expected for the inverse energy-cascade regime of two-dimensional turbulence and also for inertial-range, three-dimensional turbulence. Instead, steeper spectra approximately consistent with a -3 power law are observed at horizontal scales smaller than 3 km for all velocity components as well as potential temperature. Shallower spectra are observed at scales longer than 6 km. For horizontal velocity and potential temperature the spectral indices at longer scales are between -1.5 and -2.0. For vertical velocity the spectrum at longer scales becomes flat. It is argued that the observed velocity and potential temperature spectra are consistent with gravity waves. At smaller scales, the shapes are also superficially consistent with a Lumley–Shur–Weinstock buoyant subrange of turbulence and/or nonlinear gravity waves. Contemporaneous spectra of ozone and N_2O mixing ratio in the 100 to 1-km wavelength range do conform to an approximately uniform $-5/3$ power law. It is argued that this may reflect interactions between gravity wave air-parcel displacements and laminar or filamentary structures in the trace gas mixing ratio field produced by enstrophy-cascading two-dimensional turbulence.

1. Introduction

Studies of data collected by commercial aircraft flying in the troposphere and lower stratosphere (altitudes $\lesssim$14 km) during the Global Atmospheric Sampling Program (GASP) revealed a $-5/3$ power law for the power spectrum of horizontal velocity as a function of horizontal wavenumber over a wide range of scales [*Gage*, 1979; *Lilly and Petersen*, 1983; *Nastrom et al.*, 1984; *Nastrom and Gage*, 1985]. Although this spectral shape is consistent with the inertial range of three-dimensional (3-D) homogeneous turbulence [*Tennekes and Lumley*, 1972], the scales at which these spectral shapes are observed (up to 1000 km) are far longer than can conceivably be associated with 3-D turbulence in the atmosphere.

Gage [1979] and *Lilly* [1983] proposed that these observations reflect upscale transfer of turbulent energy that has been "two-dimensionalized" by atmospheric stratification. This interpretation was based, at least in part, on laboratory studies of stratified turbulence [e.g., *Lin and Pao*, 1979], which showed that initially-homogenous, 3-D turbulence in a stratified tank was rapidly transformed into quasi-2-D motion with predominantly vertical vorticity. In 2-D turbulence, kinetic energy injected at a certain scale will cascade to larger scales while enstrophy cascades to smaller scales [*Kraichnan*, 1967]. This results in a kinetic energy spectrum obeying a $-5/3$ power law for scales longer than the scale of the injection, while a -3 power law holds for scales smaller than the injection scale. In the picture proposed by Gage and Lilly, energy is injected into 2-D mesoscale turbulence by even smaller-scale 3-D motions (e.g. convective bubbles) which have been flattened by stratification forces. A similar process is thought to operate at much larger scales where energy is injected into 2-D turbulence at scales $\sim$5000 km by baroclinic waves [*Charney*, 1971]. This results in a kinetic energy spectrum obeying a -3 power law at scales shorter than $\sim$5000 km. Given continuous energy input, the upward-cascading energy from small-scale energy injections proposed by Gage and Lilly should encounter the downward cascading enstrophy from the large-scale inputs at some intermediate length scale. Spectra determined from the longest flights in the GASP data do in fact show a change in slope from -3 to $-5/3$ at scales $\sim$1000 km [*Nastrom and Gage*, 1985; *Gage and Nastrom*, 1985]. Horizontal wavenumber spectra for vertical velocities were not presented by the GASP investigators. Theoretical predictions for the vertical velocity spectrum based on 2-D mesoscale turbulence theories are not available.

Earlier studies found steeper spectral indices for horizontal velocities at smaller horizontal scales within

[1]Naval Research Laboratory, Washington, D.C.
[2]Computational Physics, Inc., Fairfax, Virginia
[3]NASA Goddard Space Flight Center, Greenbelt, Maryland
[4]NASA Ames Research Center, Moffet Field, California
[5]NOAA Aeronomy Lab., CIRES, Univ. of Colorado, Boulder
[6]NASA Jet Propulsion Laboratory, Pasadena, California

Paper number 95JD03835.
0148-0227/96/95JD-03835$05.00

Report Documentation Page

Form Approved
OMB No. 0704-0188

1. REPORT DATE	2. REPORT TYPE	3. DATES COVERED
APR 1996		**00-00-1996 to 00-00-1996**

4. TITLE AND SUBTITLE	5a. CONTRACT NUMBER
Stratospheric horizontal wavenumber spectra of winds, potential temperature, and atmospheric tracers observed by high-altitude aircraft	5b. GRANT NUMBER
	5c. PROGRAM ELEMENT NUMBER
6. AUTHOR(S)	5d. PROJECT NUMBER
	5e. TASK NUMBER
	5f. WORK UNIT NUMBER
7. PERFORMING ORGANIZATION NAME(S) AND ADDRESS(ES) **Naval Research Laboratory,E.O. Hulburt Center for Space Research,Washington,DC,20375**	8. PERFORMING ORGANIZATION REPORT NUMBER
9. SPONSORING/MONITORING AGENCY NAME(S) AND ADDRESS(ES)	10. SPONSOR/MONITOR'S ACRONYM(S)
	11. SPONSOR/MONITOR'S REPORT NUMBER(S)

12. DISTRIBUTION/AVAILABILITY STATEMENT
Approved for public release; distribution unlimited

13. SUPPLEMENTARY NOTES

14. ABSTRACT
see report

15. SUBJECT TERMS

16. SECURITY CLASSIFICATION OF:			17. LIMITATION OF ABSTRACT	18. NUMBER OF PAGES	19a. NAME OF RESPONSIBLE PERSON
a. REPORT **unclassified**	b. ABSTRACT **unclassified**	c. THIS PAGE **unclassified**	**Same as Report (SAR)**	**30**	

strongly stratified environments, such as above a low-level inversion [*Koprov*, 1965; *Myrup*, 1968; *Berman*, 1976] and in the upper troposphere and lower stratosphere [*Shur*, 1962, 1971; *Vinnichenko et al.*, 1965; *Lilly and Lester*, 1974]. These studies reported spectra with indices closer to -3 than $-5/3$ when strong stratification was present. *Nastrom et al.* [1987] found intensification and similar steepening of GASP spectra at large wavenumbers over mountainous terrain. Horizontal wavenumber spectra of vertical velocities were also presented in some of these studies [*Koprov*, 1965; *Myrup*, 1968; *Shur*, 1971] and were found to have spectral indices at small scales similar to those of the horizontal-velocity spectra. The explanation proposed for these findings was that strong stratification led to significant loss of energy as turbulent motions worked against buoyancy forces. This "buoyant subrange" of turbulence was proposed initially by *Bolgiano* [1962] ,*Shur* [1962], and *Lumley* [1964]. Power law spectra $\sim k^r$ were predicted, where k is the scalar wavenumber, and anticipated spectral indices r ranged between $-11/5$ [*Bolgiano*, 1962] and -3 [*Lumley*, 1964], with the latter value more widely cited. *Weinstock* [1978] later argued that a universal slope does not exist for buoyancy–modified turbulence, and derived a complex expression for the spectral energy density which depends on the flux Richardson number and the local rms velocity fluctuations. A wider range of spectral indices, $-4/3 > r > -3$, was obtained than in the earlier studies. *Weinstock* [1985] and *Dalaudier and Sidi* [1987] developed the theory of potential energy and temperature spectra in the buoyant subrange and predicted spectral indices around -3.

At intermediate to small scales (1–100 km), motions which are thought to be gravity waves are frequently detected in stratospheric aircraft data [e.g., *Lilly and Lester*, 1974; *Nastrom et al.*, 1987; *Gary*, 1989; *Bacmeister et al.*, 1990ab, 1994; *Danielsen et al.*, 1991; *Nastrom and Fritts*, 1992; *Pfister et al.*, 1993; *Chan et al.*, 1993; *Alexander and Pfister*, 1995]. Several of these studies examined statistical enhancements in variance over orography detected by aircraft [*Nastrom et al.*, 1987; *Bacmeister et al.*, 1990b; *Nastrom and Fritts*, 1992]. The remaining studies examined individual wave events associated with clearly identifiable forcing from orography or convection. Spectral analyses of airborne lidar measurements of mesospheric variability have been found to be consistent with a gravity wave interpretation [e.g., *Fritts et al.*, 1989; *Kwon et al.*, 1990; *Hostetler and Gardner*, 1994]. However, the relative contributions of gravity waves, large-scale motions, and 2-D and 3-D turbulence to stratospheric horizontal wavenumber spectra are still not clear [e.g., *Nastrom et al.*, 1987]. In this study we will attempt to to characterize the climatological structure of variablility in the lower stratosphere using high-resolution meteorological and trace gas measurements. We will attempt to determine the importance of gravity wave motions versus 2-D and 3-D turbulent motions in producing this variablilty.

2. Data and Methods

2.1 Description of Data

In this study we will compute spectra of horizontal and vertical velocities, potential temperatures, and ozone and N_2O mixing ratios, using data obtained in the midstratosphere during three aircraft campaigns employing NASA's ER-2 aircraft. The three campaigns are (1) the second Arctic Airborne Stratospheric Expedition (AASE II), (2) the Stratospheric Photochemistry Aerosol and Dynamics Experiment (SPADE), and (3) the Airborne Southern Hemisphere Ozone Experiment/Measurements for Assessing the Effects of Strato-

Table 1. Aircraft Missions

Designation	Dates	Primary Bases	ER-2 Flights
Stratosphere-Troposphere Exchange Project Tropical Experiment (STEP)	Jan.-Feb. 1987	Darwin, Australia (30°S, 131°E)	17
Airborne Antarctic Ozone Experiment (AAOE	Aug.-Oct. 1987	Punta Arenas, Chile(53°S, 70°W)	17
Airborne Aircraft Stratospheric Expedition (AASE II)	Dec. 1988 to March 1989	Stavanger, Norway(59°N, 6°E)	16
Airborne Aircraft Stratospheric Expedition II (AASE II)	Oct. 1991 to March 1992	Fairbanks, Alaska (65°N,147°W) Bangor, Maine (45°N, 69°W)	26
Stratospheric Photochemistry, Aerosol , and Dynamics Experiment (SPADE)	April-May 1993	Moffet Field, California (37°N,122°W)	10
Airborne Southern Hemisphere Ozone Experiment and Measurements for Assessing the Effects of Stratospheric Aircraft (ASHOE/MAESA)	Feb.-Nov. 1994	Barbers Point, Hawaii (21°N,158°W) Nadi, Fiji (18°S,177°E) Christchurch, New Zealand (44°S,173°E)	37

References describing these campaigns are STEP/Tropical [*Russell et al.*, 1993], AAOE [*Tuck et al.*, 1989], AASE [*Turco et al.*, 1990], AASE II [*Anderson and Toon*, 1993]

spheric Aircraft (ASHOE/MAESA). The dates and locations of these and three earlier aircraft campaigns employing the ER-2 are summarized in Table 1. Maps showing each of the ER-2 flight tracks during AASE II, SPADE, and ASHOE/MAESA are displayed in Figure 1.

We use high resolution data (sampling frequency $\gtrsim 1$ Hz) from the approximately 70 ER-2 flights conducted during AASE II, SPADE, and ASHOE/MAESA. A comparable amount of data was available from the three earlier missions (Table 1). However, improvements in instrumentation after AASE led us to focus on the latest three missions. To our knowledge, this is the most extensive single data set available for studies of mesoscale motions in the middle stratosphere. The ER-2's cruising altitude is close to 20 km or 60,000 ft, which is 20,000–30,000 ft higher than the commercial airliners used in the GASP investigations. Pressures below 70 mbar are reached routinely, and measured Brunt-Väisälä frequencies routinely exceed 0.020 rad s^{-1} [e.g. *Gary*, 1989]. The data set has a definite bias toward wintertime polar and mid-latitude conditions, since the primary objective of four of the six missions was to examine polar ozone chemistry. However, during AASE II and SPADE equatorward flights were conducted regularly, and during ASHOE/MAESA two out of every six deployments took place from Hawaii (see Figure 1). Thus approximately one third of the flights examined here sampled tropical air.

Velocity, temperature, and pressure data were measured from the ER-2 by the Meteorological Measurement System (MMS) [*Scott et al.*, 1990]. MMS makes in situ measurements of the three-dimensional vector wind velocity, as well as temperature and pressure, at a sampling frequency of 5 Hz. Ozone measurements were obtained by the NOAA dual-beam ozone photometer [*Proffit et al.*, 1989] at a sampling frequency of 1 Hz. We also examine measurements of N_2O taken by the airborne tunable laser absorption spectrometer (ATLAS) [*Loewenstein et al.*, 1989; *Podolske et al.*, 1989]. ATLAS measurements were recorded at 1 Hz. However, instrument noise appears to dominate the signal for frequencies higher than 0.3-0.5 Hz [*Strahan and Mahlman*, 1994]. We use the data as reported, but caution is required when interpreting the highest frequency signals in the N_2O data

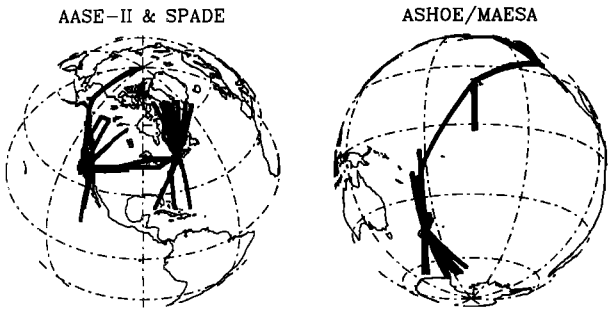

Figure 1. (Left) Map showing ER-2 flight tracks for AASE II and SPADE aircraft campaigns. Flights during these two campaigns were launched from Fairbanks, Alaska; Moffet Field, California; and Bangor, Maine. (Right) Map showing ER-2 flight tracks for ASHOE/MAESA campaign. Flights originated from Moffet Field, California; Barbers Point, Hawaii; Nadi, Fiji; and Christchurch, New Zealand.

For purposes of characterizing the meteorological conditions in which measurements were taken, we used temperature profile data from the microwave temperature profiler (MTP) [*Gary*, 1989; *Denning et al.*, 1989] as well as global meteorological analyses of wind and temperature obtained from the National Meteorological Center Climate Analysis Center (NMC/CAC) [*Newman et al.*, 1993]. The MTP provides 15 independent temperature measurements within a layer extending about 3 km above and below the aircraft's altitude. The temperature profiles are converted to potential temperature using pressures derived from the hydrostatic relation [*Gary*, 1989]. A complete profile is obtained every 14 s. The NMC data are obtained daily at 1200 UT on a global grid at a resolution of $5° \times 2°$ on 18 standard pressure levels. These data are interpolated in all three spatial dimensions as well as in time onto each of the ER-2 flight tracks flown during AASE II, SPADE, and ASHOE/MAESA. Figure 1 shows maps of each of the ER-2 flight tracks executed during AASE II, SPADE, and ASHOE/MAESA.

2.2 Wavelet Transforms

Our analysis of the aircraft data employs wavelet transforms rather than Fourier transforms. Orthonormal wavelets are families of orthogonal functions which, unlike sines and cosines, are localized in both the spatial and wavenumber domains [*Daubechies*, 1988; *Mallat*, 1989]. A large number of families of orthonormal wavelets has been identified. Some are compactly supported (i.e. exactly equal to zero outside of a finite interval), while others approach zero asymptotically outside of a finite interval. In the following analysis, we use the discreet wavelet transform (DWT) described by *Press et al.* [1992]. This algorithm can accommodate any compactly supported wavelets for which filter coefficients are known. We use the six-coefficient member of the wavelet class identified by *Daubechies* [1988]. An example of this wavelet can be seen in Figure 2a.

Due to the localization of the basis functions, DWT spectra contain information about the location of variability in the time series as well as its frequency. The DWT spectrum is most easily interpreted when broken down into its component "octaves". At each octave the DWT shows variability at a specific frequency or wavenumber as a function of location. Adjacent octaves show frequencies separated by factors of 2. Figures 2b-2d show the DWT of the "data" in Figure 2a broken down into some of its component octaves. An obvious relationship exists between the peaks in the DWT spectrum and the localized variability in the data. Unfortunately, for a data sequence with 2^N elements, only N octaves can be obtained. Thus, the price for the spatial information contained in the DWT is a significant loss of frequency resolution when compared to a fast Fourier

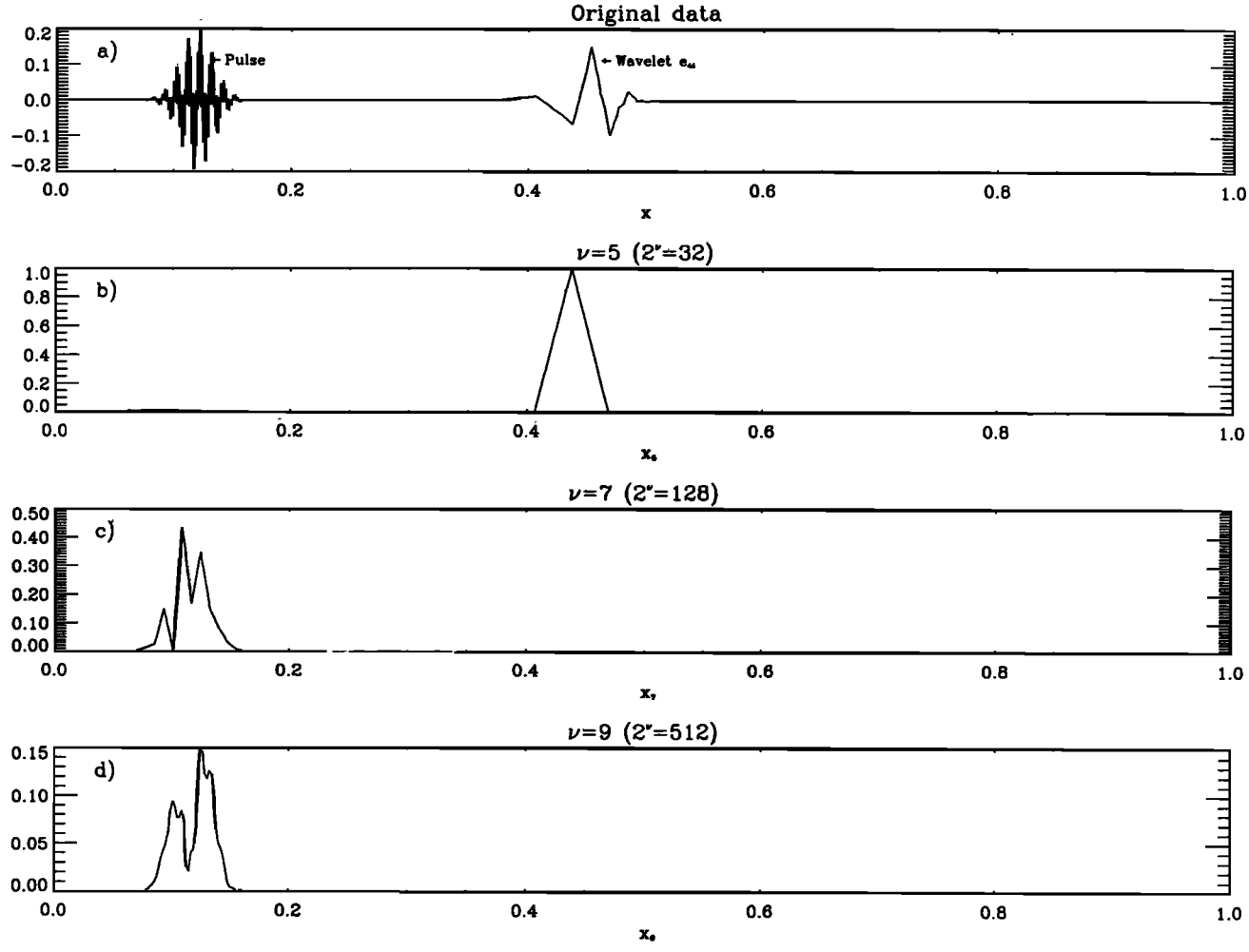

Figure 2. (a) Artificial data sequence consisting of a high-frequency Gaussian-modulated pulse described by $e^{-(x-0.12)^2/0.02^2}[\sin(200\pi x)+\sin(1000\pi x)]$ and a Daubechies (6) wavelet at x =0.35-0.5. The wavelet is the inverse transform of the unit vector e_{44} , i.e., zeros everywhere except for the 44th element, which is 1. Since 44 lies between $2^5 = 32$ and $2^6 = 64$ the peak in the forward transform occurs in fifth octave at a position close to $x = 3/8 \pm 3/32$, where the uncertainty results from arbitrariness in the positioning of the six element filter. (b) The fifth octave ($\nu = 5$) of the DWT of the data in Figure 2a. (c) As in Figure 2b, except for $\nu = 7$. (d) As in Figure 2b, except for $\nu = 9$.

transform(FFT). However, when plotted on logarithmic axes, as we will do later, the DWT frequencies are equispaced, and the degraded frequency resolution is no longer a serious drawback.

The advantages of DWTs over FFTs are greatest for sequences of data which are characterized by large intermittent events. In this case, DWTs provide a straightforward connection between features in the original data and spectral features. This is clearly seen in Figure 2. DWTs were chosen for this analysis because we expected the aircraft data to consist primarily of intermittent high-energy peaks in variance associated with isolated wave or turbulence events. This supposition is based on previous studies of atmospheric wind measurements using aircraft [e.g.,*Nastrom et al.*, 1987; *Yamada and Ohkitani*, 1991; *Nastrom and Fritts*, 1992; *Bacmeister et al.*, 1994].

DWTs also offer several procedural advantages over FFT's. Application of windows to the data to mitigate edge effects is unnecessary. Edge effects can be simply accounted for by ignoring DWT components located near the edge of the original data sequence. Similarly, the possibility of artificial variability induced by aircraft maneuvers (e.g., dives, box turns) is easily assessed by examination of the DWT in the vicinity of the maneuvers. However, it should be emphasized that none of the results presented in this study depend crucially on the use of DWTs instead of FFTs, nor does the particular choice of wavelet function significantly affect the results.

2.3 Determination of Power Spectral Densities From DWTs

Results of earlier studies of small-scale variability in the atmosphere are typically presented in terms of averaged power spectra. The most important quantity derived from these spectra is usually the mean slope of the spectra in log-log coordinates, i.e., the spectral index. For comparison of our DWT spectra with Fourier power spectra presented in earlier studies, we must first define a mean DWT power spectrum for our aircraft data as a function of frequency or wavenumber. We do this following the procedure outlined by *Yamada and Ohkitani* [1991] and *Katul et al.* [1994].

A typical ER-2 flight during the AASE II, SPADE, or ASHOE/MAESA missions was 6-8 hours long. The input data for the DWT analysis consist of 5-Hz MMS temperature, pressure and wind velocity measurements, which have been bin-averaged onto a uniform 1-s time grid, and the original 1-Hz NOAA ozone and ATLAS N_2O measurements. Thus the complete time series of each quantity for each flight is typically ~25,000 elements long. Infrequent data gaps were filled using linear interpolation.

We calculate average DWT power spectra for subintervals of data lasting 1024 s, so that 20 to 25 spectra are typically obtained for each quantity for each flight. First, the DWT spectrum is calculated for the jth 1024-element data segment, $X_j(t)$,

$$X_j(t) \rightarrow \text{DWT} \rightarrow [D_{j,0}, D_{j,1}, ..., D_{j,9}] = [D_{j,\nu}],$$

where $\nu = 0, ..., 9$. The $D_{j,\nu}$ denote the 10 separate octaves ν of the DWT of $X_j(t)$, each containing 2^ν elements. These are used to calculate an average DWT squared-amplitude within each octave for $X_j(t)$,

$$WT_j(\nu) = \left(\frac{1}{2^\nu}\right) \sum_{i=1}^{2^\nu} D_{j,\nu}^2(i). \quad (1)$$

A mean-squared wavelet amplitude is thus defined for each of the 10 octaves which can be obtained from a 1024-element time series. The index of the octave, ν, corresponds roughly to $\log_2(\Omega)$, where Ω is the frequency of the FFT spectrum. Fourier modes with frequencies $\Omega = 2^\nu$ have DWT power spectra which peak sharply at the kth octave. Fourier modes for which $2^{\nu-1} < \Omega < 2^\nu$ project power onto the two bracketing octaves ν and $\nu - 1$.

The total number N_{sp} of individual DWT power spectra obtained for each measured quantity varies between 1290 and 1680, when the entire data set of 73 or so flights is used. Differences in the number of individual spectra for the various quantities are due to occasional payload changes, varying on-off times for different instruments, data reduction failures, and instrument failures. The more than 1000 individual DWT spectra for each quantity can be log-averaged to give an average power spectrum for the entire data set,

$$\log_2[\overline{WT}^{\text{set}}(\nu)] = \left(\frac{1}{N_{sp}}\right) \sum_{j=1}^{N_{sp}} \log_2[WT_j(\nu)]. \quad (2)$$

This average DWT power spectrum is comparable to the average FFT power spectral densities presented in

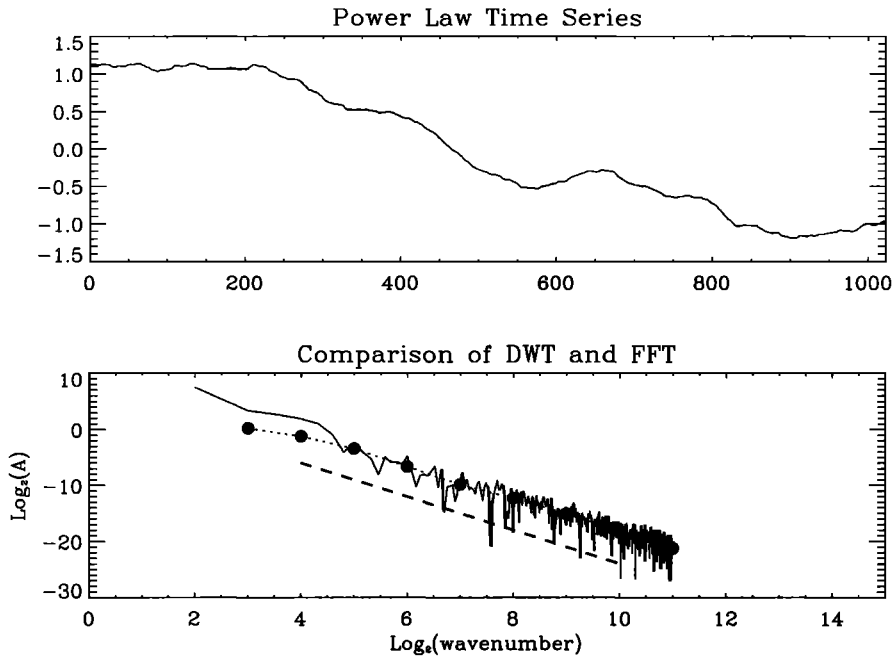

Figure 3. (top) Segment of an artificial power law time series with energy or variance $\sim k^{-3}$. (bottom) Comparison of power spectral densities (PSD) for the data in Figure 3 (top) obtained from a windowed FFT (solid line) and a DWT (solid circles). The expected −3 slope is indicated by the thick dashed line.

other studies. Average power spectra for subsets of the data are calculated in an analogous manner.

In order to test this procedure, we applied it to a 1024-element subinterval of an artificially generated, 4096-element aircraft time series,

$$Y(t) = \sum_{\Omega=1}^{2048} \Omega^{-1.5} \sin[\Omega t + \phi(\Omega)]$$

where t represents the interval $[0, 2\pi]$ divided into 4096 segments and $\phi(\Omega)$ is a random phase between 0 and 2π. Results are shown in Figure 3. An FFT power spectrum of the same time series is shown for comparison. The spectral index, or slope of the DWT power spectrum in log-log coordinates, agrees well with the analytical spectral index of -3. The average slope of the FFT power spectrum in log-log coordinates is also close to -3. The scatter or "structure" visible in the FFT spectrum results entirely from the application of a triangular (Bartlett) window to the data before calculating the power spectrum. This is necessary in practice to reduce contamination of the computed FFT spectrum by edge effects.

In the following analysis, the approximate mean ER-2 airspeed of 200 m s^{-1} is used to transform timescales in the data into spatial scales via a straightforward Taylor transformation. While a standard method in the presence of turbulence, Taylor's hypothesis is not automatically valid in the presence of wave motions, which propagate relative to the background wind. In section 4 it will be shown that Taylor's hypothesis does not introduce significant errors for the gravity wave spectra that are typically encountered at these heights. Thus we assume that a feature in the aircraft time series with a period of 1024 s possesses a horizontal wavelength of 204.8 km, while a feature at our resolution limit of 2 s possesses a wavelength of 400 m. For direct comparison with FFT power spectral densities (PSDs) shown in previous studies, we scale the mean-squared wavelet amplitudes in (1) and (2) as in the work by *Katul et al.* [1994]:

$$E(\nu) = \left(\frac{\Delta s}{2\pi \ \ln(2)}\right) WT(\nu)$$

where $WT(\nu)$ can represent either the individual DWT squared-amplitudes in (1) or the log - averaged amplitudes in (2) and Δs represents the distance covered by the aircraft between samples. We use $\Delta s \approx 200$ m. $E(\nu)$ is now directly comparable to Fourier power spectral densities calculated in earlier studies of atmospheric horizontal wavenumber spectra.

3. Results

3.1 Average Spectra of Velocities and Potential Temperature

Figure 4a shows DWT power spectral densities $E(\nu)$ of horizontal and vertical velocities, log-averaged over the entire data set. The set-averaged power spectrum of potential temperature is shown in Figure 4b. Spectral indices (slopes) are significantly steeper than $-5/3$ for scales shorter than 6 km ($\nu > 5$) for all wind components as well as for potential temperature. The spectral slopes at these scales appear to be closer to -2.5 or -3. At wavelengths between 6 and 25 km the spectrum of both horizontal velocity components flattens, and at larger scales approaches the more familiar $-5/3$ law reported in studies using the GASP data set [*Nastrom et al.*, 1984; *Nastrom and Gage*, 1985] and other studies using radar [e.g. *Gage and Nastrom*, 1985]. Analyses of higher-resolution GASP data [*Nastrom et al.*, 1984; *Nastrom and Gage*, 1985] returned indices of approximately $-5/3$ down to scales of 2 km.

Thus the average spectra in Figure 4 appear to disagree with the GASP results at horizontal scales below about 25 km. Later, more detailed analysis by *Nastrom et al.* [1987] found increased spectral powers and spectral indices near -3 at large wavenumbers in GASP spectra measured over mountainous terrain in high wind conditions. The GASP spectra under these conditions are similar to the set-averaged spectra shown in Figure 4. However, the GASP climatological mean spectrum under normal meteorological conditions retained a spectral index close to $-5/3$ down to scales of 2 km [*Nastrom et al.*, 1987]. The average spectra shown in Figure 4 contain measurements made in a variety of meteorological conditions. As can be seen in Figure 1, a large fraction (in fact well over half) of the ER-2 flight time for which we have data occurred over oceans. Thus it appears unlikely that the agreement between our average spectra and the high-wind, high-topography spectra examined by *Nastrom et al.* [1987] is due to a topographic bias in our data. In section 3.3 we will examine in more detail the effect of several meteorological variables on our average spectra.

At high wavenumbers the average velocity spectra in Figure 4a resemble some of those derived from other high-resolution data sets obtained using specially instrumented aircraft [*Shur*, 1962, 1971; *Vinnichenko et al.*, 1965; *Koprov*, 1965; *Myrup*, 1968; *Lilly and Lester*, 1974]. *Vinnichenko et al.* [1965] and *Shur* [1971] described a series of experiments conducted over central Asia (Uzbekistan) [*Vinnichenko et al.*, 1965] and the Caucasus Mountains [*Shur*, 1971]. In these studies aircraft were flown at several altitudes between the lower troposphere and the tropopause. Horizontal velocity spectra with spectral indices between $-5/3$ and -3 were obtained for scales down to 500 m. The steeper spectral slopes were invariably associated with high ambient stratification. *Lilly and Lester* [1974] described a series of flights over the Sangre de Cristo Mountains in Colorado at altitudes of 13-20 km. All of the horizontal velocity spectra measured during these flights had indices of approximately -3 down to the reported resolution limit of 2 km. *Koprov* [1965] and *Myrup* [1968] described separate aircraft experiments conducted in strong, low-level, nocturnal inversions over flat desert terrain in central Asia [*Koprov*, 1965] and over a dry lake bed in northern California [*Myrup*, 1968]. In each

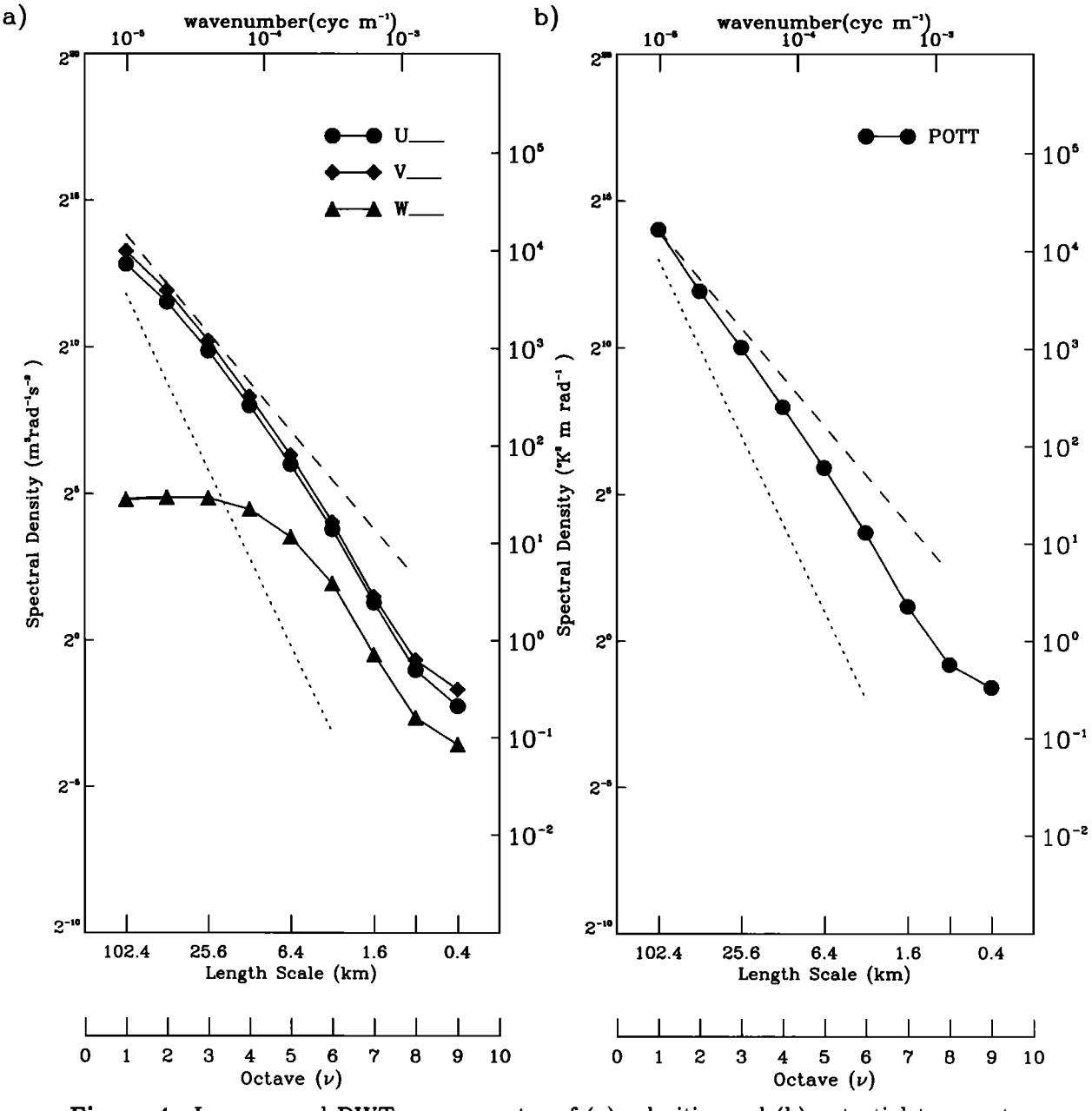

Figure 4. Log-averaged DWT power spectra of (a) velocities and (b) potential temperature. Log averages are taken over the entire set of available 1024-s spectra of each quantity. (a) Solid circles show log-averaged spectrum of zonal velocity, solid diamonds show meridional velocity, and solid triangles show vertical velocity. Short dashed shows a -3 slope. Long dashed line shows a $-5/3$ slope.

of these experiments, kinetic energy spectra with indices near -3 were measured during the early morning while the inversion was strong. As the inversion was destroyed by solar heating, the indices of the measured kinetic energy spectra approached $-5/3$. Finally, *Berman* [1976] reported horizontal-velocity frequency spectra $\sim\Omega^{-3}$ measured by a ship-based, tethered balloon at the top of a stable marine boundary layer.

In each of the studies just described, spectra with slopes steeper than $-5/3$ were obtained only in atypical geographical or meteorological environments. However, the stratospheric meteorological data collected from the ER-2 appear to yield spectra with slopes close to -2.5 under general conditions. A randomly-chosen subset of individual power spectra for 1024-s segments of zonal velocity (U) data is shown in Figure 5. The individual spectra tend to lie within a fairly narrow band around the average power spectrum of U in Figure 4a. To make this characterization more quantitative and to assess the statistical significance of our slope estimates, we examine the distribution of slope values obtained at each octave for each of the $N_{sp} > 1000$ individual 1024-s DWT power spectra of each quantity.

The value of the spectral index between the νth oc-

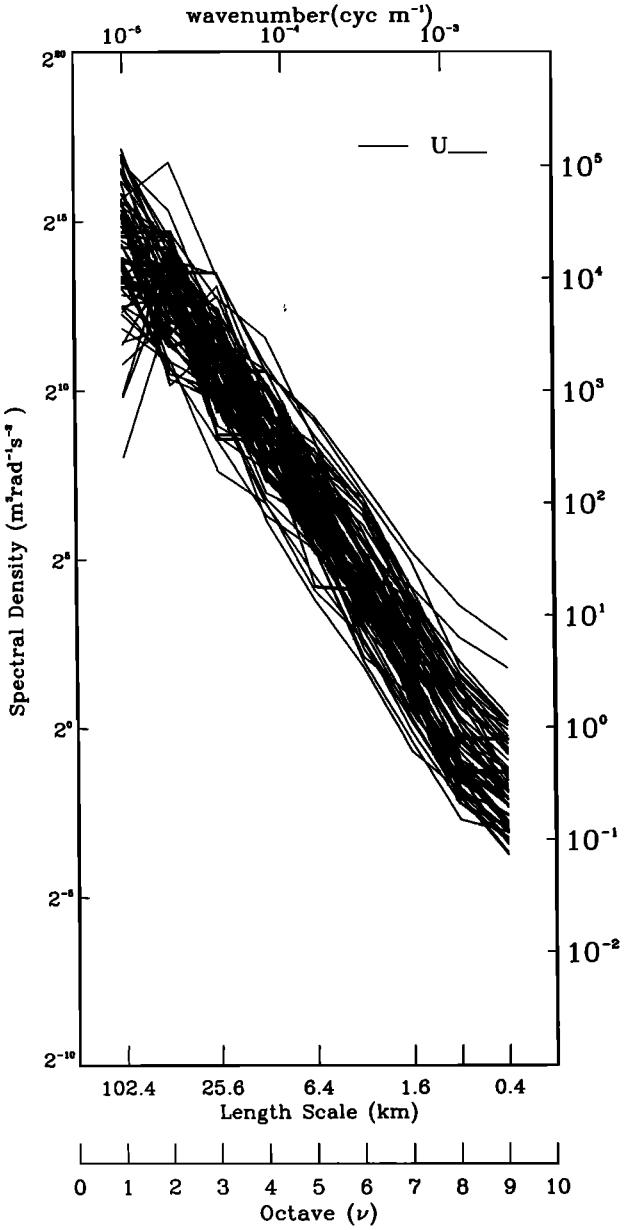

Figure 5. Randomly selected subset of individual DWT power spectra for 1024-s segments of zonal wind data from MMS. Note the relatively tight concentration of the lines. This suggests that the mean spectrum in Figure 4a is robust.

tave and the $(\nu+1)$th octave for each individual spectrum is given by,

$$S_j(\nu+1/2) = \log_2[E_j(\nu+1)] - \log_2[E_j(\nu)] \quad (3)$$

where $E_j(\nu)$ is the average power of the νth octave of the DWT for the jth data segment as defined in (1). There is a denominator implicit in (3) which measures the change in log-frequency or log-wavenumber, Ω, between octaves $\nu+1$ and ν, but is simply equal to 1 since $\Omega(\nu) \sim 2^{\nu}$. Figure 6 shows histograms of slope values S_j of U at each octave for the entire data set. The histograms are sharply peaked, particularly at higher octaves . The histograms for $\nu + 1/2 = 5.5, 6.5$ and 7.5 have peaks between -2.33 and -2.66 with few occurrences of slopes flatter than $-5/3$. The histograms strongly suggest that the mean spectral slopes for horizontal velocity in this data set at scales below 25 km are in fact significantly steeper than $-5/3$. Table 2 shows mean values and 80% confidence limits for the slope histograms of U in Figure 6, as well as confidence limits for slope histograms of the other quantities examined.

The mean power spectrum of vertical velocity (Figure 4a) differs markedly from those of the other meteorological quantities examined here. At scales of 3 km and shorter ($\nu > 6$) the slope of the spectrum is near -2.4, which is similar to the slope of the horizontal velocity spectra at these scales. This agreement would be consistent with an explanation based on homogeneous buoyancy–modified turbulence in which the power spectrum of all velocity components decays as k^{-r}, where r is between 4/3 and 3, [e.g., *Lumley*, 1964; *Weinstock*, 1978, 1985a]. In fact, vertical velocity spectra with observed k^{-3} behavior at scales 0.5–5 km were reported by *Koprov* [1965], *Myrup* [1968], and *Shur* [1971].

However, at scales longer than 6 km the slope of our average power spectrum for vertical velocity flattens out rapidly and above 25 km the spectrum is essentially flat. The histogram analysis of the slopes (Table 2) again suggests that slope estimates are relatively robust. This flattening out of the vertical velocity power spectrum at large scales simply reflects the intuitively obvious fact that strong, mesoscale updrafts and downdrafts do not exist in the mean atmosphere. However, to our knowledge this necessary feature of the vertical velocity wavenumber spectrum has not been observed by previous aircraft studies.

Interestingly, ST radar measurements of vertical velocities yield spectra with spectral indices close to 0 at low frequencies [*Ecklund et al.*, 1986; *VanZandt et al.*, 1991]. In these studies, the vertical velocity spectrum typically posesses a steep high-frequency tail, while exhibiting nearly constant power (i.e., spectral index 0) for measured periods longer than 10-30 min. A rigorous treatment of these spectra involves the consideration of Doppler shifting effects and Taylor transformations, in order to identify their dynamical content [*Gage and*

Figure 6. Histograms showing distribution of slopes for each octave for all individual horizontal wind DWT power spectra in the data set. (a) Histogram of slope values between octaves 1 and 2, or roughly speaking, for horizontal scales between 102.4 km and 51.2 km. (b) Same as Figure 6a for octaves 2 and 3, and horizontal scale between 51.2 and 25.6 km . (c) Octaves 3 and 4, horizontal scale between 25.6 and 12.8 km. (d) Octaves 4 and 5, horizontal scale between 12.8 and 6.4 km. (e) Octaves 5 and 6, horizontal scale between 6.4 and 3.2 km. (f) Octaves 6 and 7, horizontal scale between 3.2 and 1.6 km. (g) Octaves 7 and 8, horizontal scale between 1.6 km and 800 m. (h) Octaves 8 and 9, horizontal scale between 800 m and 400 m.

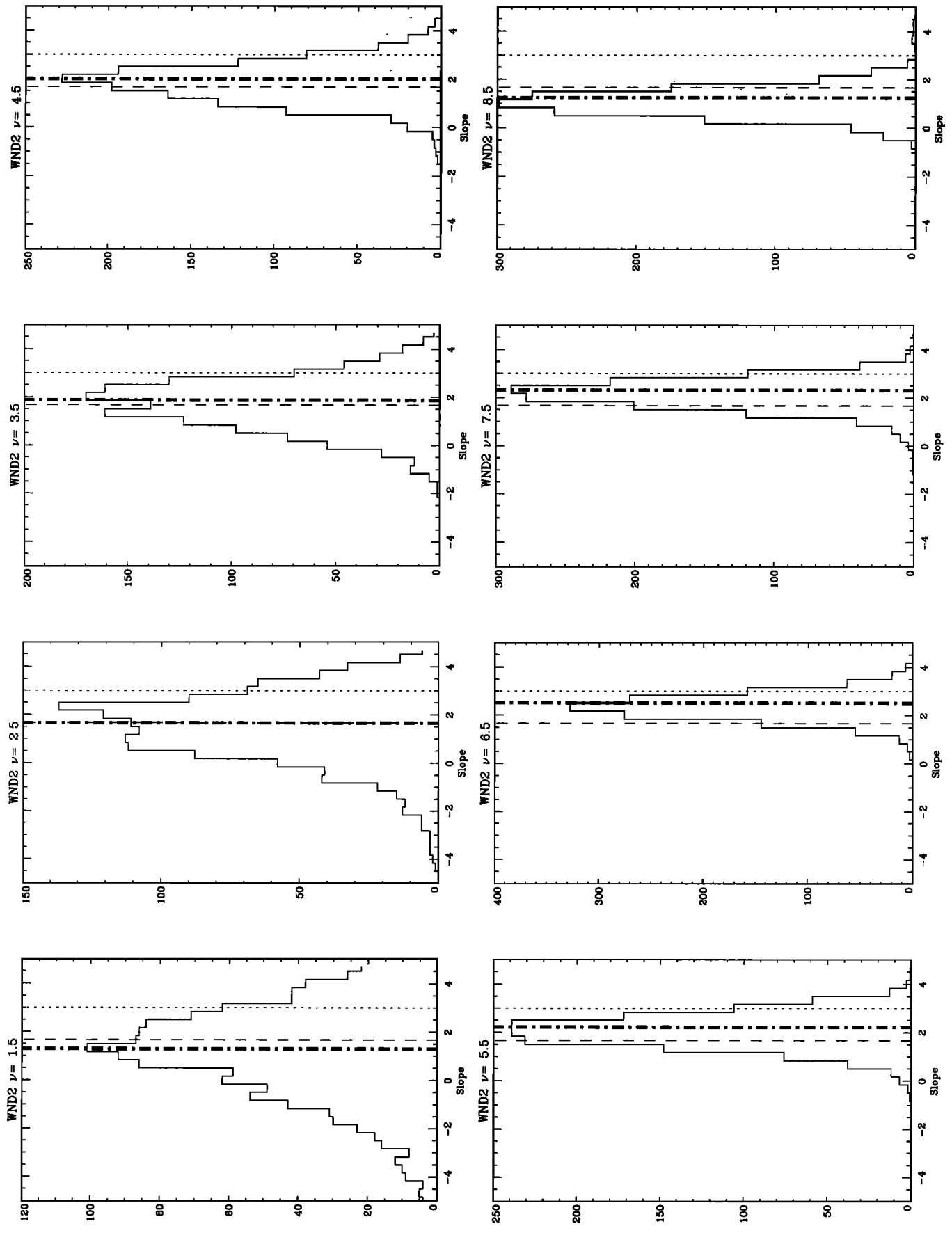
WND2 ν= 4.5
WND2 ν= 8.5
WND2 ν= 3.5
WND2 ν= 7.5
WND2 ν= 2.5
WND2 ν= 6.5
WND2 ν= 1.5
WND2 ν= 5.5
Slope

Table 2. Spectral Indices

Octave	10th Percentile	Mean	90th Percentile	n
		Zonal Velocity		1348
2.5	+0.17	-1.66	-3.17	
4.5	-0.83	-1.99	-2.83	
6.5	-1.83	-2.51	-2.83	
		Meridional Velocity		1348
2.5	+0.50	-1.70	-3.17	
4.5	-0.83	-1.99	-2.83	
6.5	-1.83	-2.55	-2.83	
		Vertical Velocity		1290
2.5	+1.83	-0.02	-3.33	
4.5	+0.17	-0.94	-1.83	
6.5	-1.50	-2.43	-2.83	
		Potential Temperature		1510
2.5	+0.17	-1.91	-3.50	
4.5	-0.83	-2.07	-2.83	
6.5	-1.83	-2.52	-2.83	
		Ozone		1639
2.5	+0.50	-1.78	-3.50	
4.5	-0.50	-1.74	-2.83	
6.5	-1.17	-2.04	-2.83	
		N_2O		1160
2.5	+0.17	-1.81	-3.50	
4.5	-0.50	-1.74	-2.83	
6.5	-0.83	-1.90	-2.83	

Results of histogram analysis of spectral slopes for each quantity examined. Slope histograms for horizontal velocity are shown in Figure 5. The table shows the 10th and 90th percentile values for the slope histograms as well as the mean value for $\nu = 2.5$, 4.5, and 6.5. The last column gives the total number of 1024-s data segments available for each quantity.

Nastrom, 1985; *Vincent and Eckermann*, 1990; *VanZandt et al.*, 1991]. A similar sort of analysis of the aircraft spectra is undertaken in Section 4.

3.2 Average Spectra of Ozone and N_2O

Figure 7 shows set-averaged spectra of ozone mixing-ratio variance and N_2O mixing-ratio variance. They are noteworthy in that they are the only spectra analyzed which appear to conform closely to the $-5/3$ power law at most scales. Slope histograms yield spectral indices close to -1.7 (Table 2). A relatively distinct transition from a $-5/3$ behavior to -2 behavior occurs in the ozone spectrum at a wavelength of 3.2 km ($\nu = 6$). However, the slope histograms (not shown) suggest that this is due more to a reduction in the relative number of spectral segments with flat slopes, rather than to a shift in the peak of the distribution of slopes. The peaks remain near $-5/3$ for all octaves, except for the highest ($\nu + 1/2 = 8.5$) octave, which may be an aliasing effect [*Eckermann*, 1990]. It is also worth noting that the spread in the slope histograms for ozone is somewhat larger than for horizontal velocity and vertical velocity. This is seen in the slightly larger spread between the 10 and 90 percentiles of the spectral index determinations for ozone and horizontal velocity given in Table 2.

The average power spectrum for N_2O conforms closely to $k^{-5/3}$ at all scales. This is consistent with the analysis of *Strahan and Mahlman* [1994], who derived spectral indices between -2 and $-5/3$ for N_2O data from the AASE and AAOE campaigns. Thus the ozone spectra and the N_2O spectra derived from the present data exhibit similar k^{-p} behavior where $1.5 < p < 2.0$ for the range of horizontal scales 100 km $\gtrsim \lambda \gtrsim$ 1 km. Thus the average power spectra of tracer variance appear to be significantly flatter than the power spectra of the dynamical quantities at these scales.

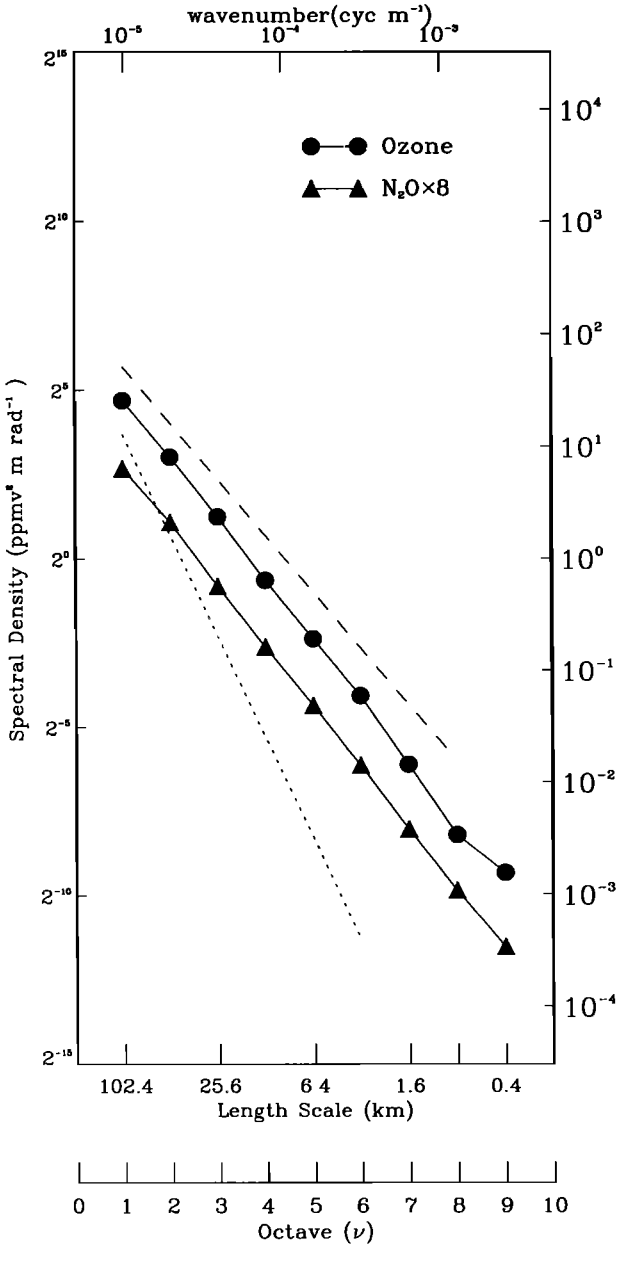

Figure 7. Log-averaged DWT power spectra of ozone and N_2O mixing ratio variance. Log averages are taken over the entire set of available 1024 s spectra of each quantity. Solid circles show log-averaged spectrum of ozone mixing ratio variance. Solid triangles show N_2O variance. Mixing ratios N_2O were arbitrarily multiplied by 8 to make them comparable to ozone mixing ratios. Short dashed line shows -3 slope. Long dashed line shows $-5/3$ slope.

3.3 Spectra Stratified According to Velocity Variance, Mean Velocity, and Stratification

Several mechanisms can be invoked to explain the steeper than expected slopes of our set-average dynamical power spectra. The possibility of turbulence in the buoyant subrange has already been mentioned. Other possibilities include spectra due to saturated or unsaturated gravity wave motions. In order to obtain possible insights into the nature of the motions creating our power spectra, we now examine the impact of several meteorological variables on the shape of the spectra obtained from our aircraft data. A similar classification of GASP spectra according to mean ambient horizontal velocity was performed by *Nastrom et al.* [1987].

Here we examine not only the influence of the mean ambient horizontal velocity on the shape of the measured spectra, but also that of mean horizontal velocity variance and mean stratification. Mean stratification is expected to affect the spectral slope if buoyancy–dominated turbulence is present [*Weinstock*, 1978; *Vinnichenko et al.*, 1980]. Mean horizontal velocity and mean horizontal velocity variance may be expected to influence the shape of a spectrum of interacting gravity waves [*Fritts and VanZandt*, 1987; *Hines*, 1991; *Eckermann*, 1995], as well as a turbulent spectrum in the 2–D or buoyant subranges [*Weinstock*, 1978; *Nastrom et al.*, 1987; *Eckermann*, 1990].

Estimates of mean horizontal velocity and rms horizontal velocity variance are obtained directly from the MMS data. Mean ambient horizontal velocity is calculated for each 1024-s interval in the data set by simply bin averaging the MMS measured horizontal velocity over the interval.

An index of rms horizontal velocity variance is obtained directly from the DWT power spectra of horizontal velocity. We simply take the log-average power over all nine octaves of the DWT power spectrum of horizontal velocity for a given 1024-s interval of data. This average is compared to the average over the entire data set to characterize unusually active or quiet periods. Estimates of the mean stratification at the time of measurement are taken from NMC analyses of potential temperature interpolated to the location and time of the measurement or from time-averaged MTP measurements of lapse rates.

Effect of horizontal velocity variance To sort spectra according to total horizontal velocity variance, first we calculate the log-averaged PSD for total horizontal velocity over all octaves for the set-averaged power spectrum shown in Figure 4a.

$$\log_2\left([\overline{E}^{\text{set}}]_{UV}\right) = \left(\frac{1}{9}\right)\sum_{\nu=1}^{9}\log_2\left(\overline{E}^{\text{set}}_{UV}(\nu)\right)$$

where the set-averaged spectrum of total horizontal velocity is given by the sum of the components, i.e., $\overline{E}^{\text{set}}_{UV} = \overline{E}^{\text{set}}_{U} + \overline{E}^{\text{set}}_{V}$. Set averages are defined by (2). From the log-averaged power spectra of zonal and meridional velocity shown in Figure 4a, we obtain $[\overline{E}^{\text{set}}]_{UV} \approx 2 \times 2^{5.6}$ m^3 rad^{-1} s^{-2}. We now calculate an analogous quantity $[E_j]_{UV}$ for each of the $N_{sp} > 1300$ individual DWT power spectra of horizontal velocity. We divide the data into two groups: an "active" group, in which $[E_j]_{UV} > 2[\overline{E}^{\text{set}}]_{UV}$, and a "quiet" group, in which $[E_j]_{UV} < \frac{1}{2}[\overline{E}^{\text{set}}]_{UV}$.

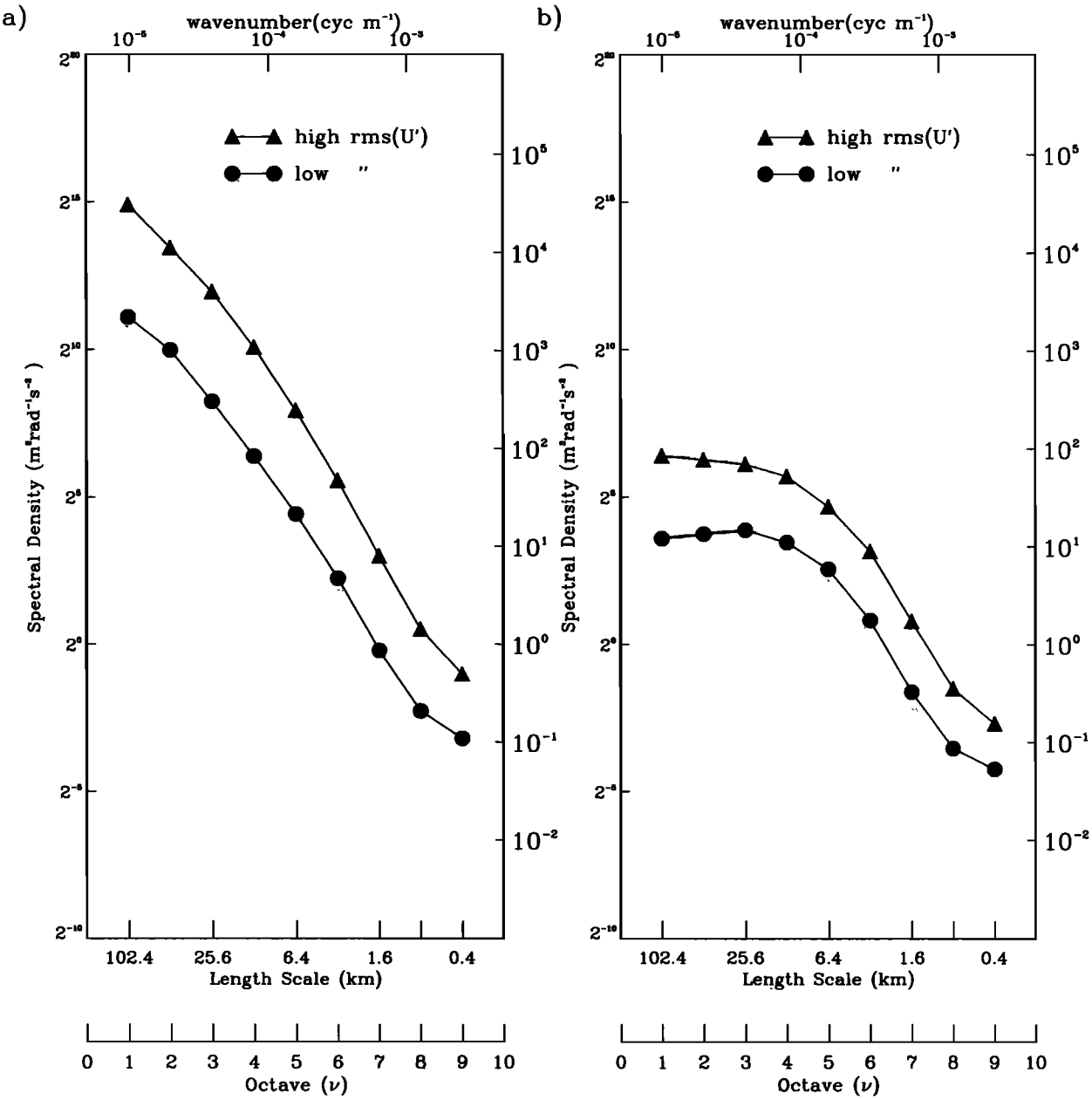

Figure 8. DWT power spectra of (a) horizontal and (b) vertical velocity sorted according to the magnitude of the horizontal velocity variance (see text). Solid triangles show average for high variability group. Solid circles show low variability group.

Figure 8 shows DWT power spectra of zonal and vertical velocity for both groups. Power spectra of vertical velocity are shown in Figure 8b. The upper curve in Figure 8b shows the log-averaged power spectrum of vertical velocity for active intervals, and the lower curve shows the log-averaged spectrum for quiet intervals. The two curves are simply offset in the vertical, and no detectable difference in the shape of the vertical velocity spectra appears to result from grouping the data in this way.

Similar sorting of the horizontal velocity spectra in Figure 8a yields a similar result. A mean vertical offset between the two curves in Figure 8a is an unavoidable result of the sorting procedure. However, there is no requirement that spectral slopes remain the same. Nevertheless, the log-averaged power spectra again appear to be nearly identical in shape except for the vertical offset. This result appears to be somewhat at odds with the theory of *Weinstock* [1978], which suggests that the shape of the kinetic energy spectrum for turbulence in the buoyant subrange should depend on the local rms velocity variance.

Effect of mean horizontal velocity The situation changes somewhat when the spectra are sorted according to the mean horizontal wind speed at the time of measurement. Again, we sort the individual spectra

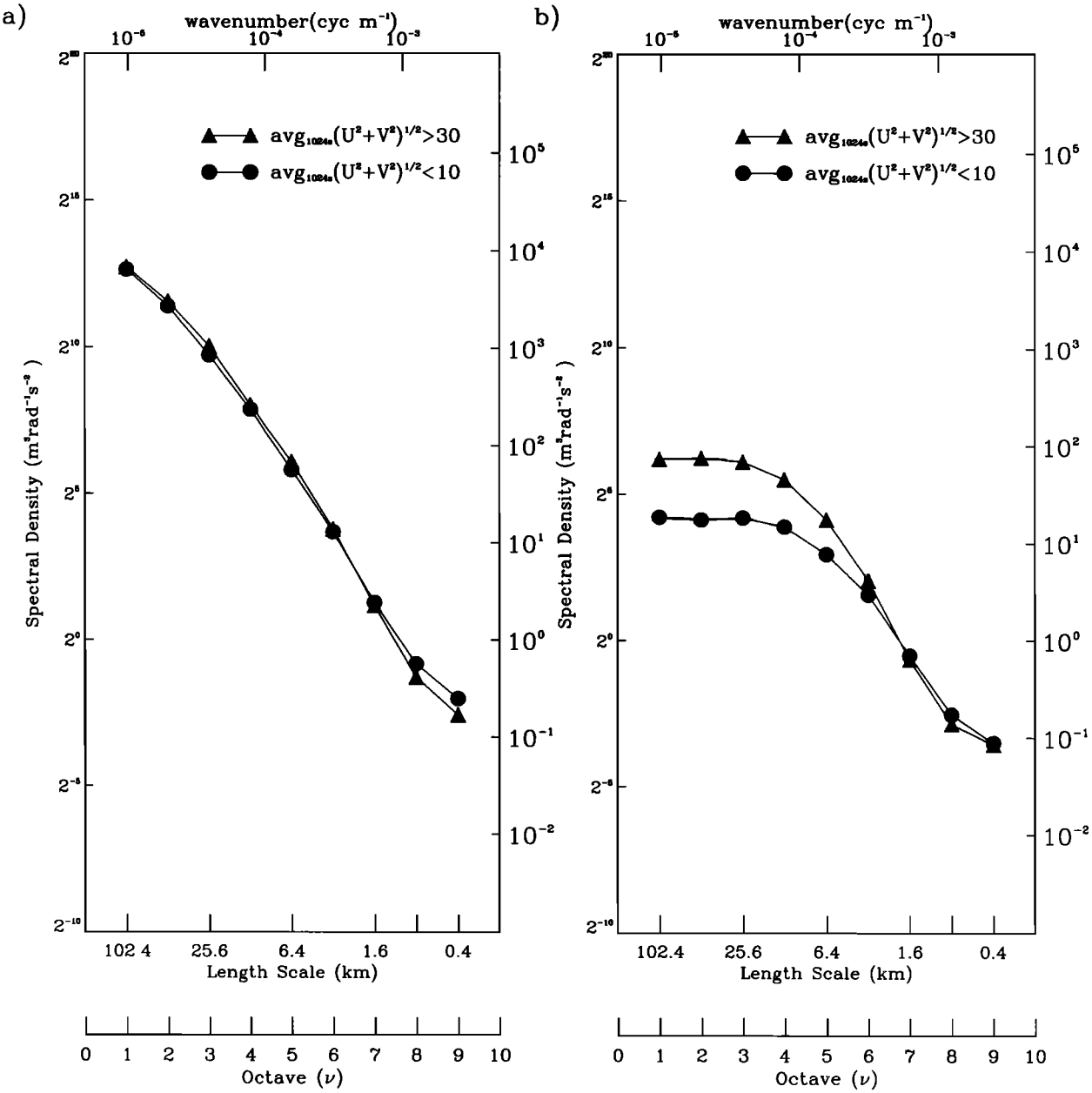

Figure 9. Log-averaged DWT power spectra of (a) horizontal and (b) vertical wind sorted according to the magnitude of mean ambient horizontal velocity (i.e., mean horizontal wind speed). Mean ambient horizontal velocity is obtained from 1024 s averages of $(U^2 + V^2)^{1/2}$ as measured by the MMS along the ER-2 flight track. Two subsets of the data are constructed: one for mean horizontal velocity <10 m s^{-1} and another for mean horizontal velocity >30 m s^{-1}. Solid triangles show average for high wind speed group. Solid circles show low wind speed group.

into two groups; one for which the corresponding 1024-s-averaged MMS horizontal wind speed is greater than 30 m s^{-1} and another for which it is less than 10 m s^{-1}. These limits were chosen to yield groups of spectra with similar numbers of members. This sorting procedure is similar to that performed by *Nastrom et al.* [1987] with the GASP data, except that they used a single velocity value of 25 m s^{-1} to separate their data into high- and low-velocity groups. In addition, unlike Nastrom et al. we do not segregate our data according to underlying topography.

Figure 9b shows log-averaged power spectra of vertical velocity for subsets of data which have been sorted according to mean horizontal velocity. In contrast to the earlier subdivision by rms horizontal velocity variance, the shape of the vertical velocity spectra does appear to change in response to varying mean horizontal wind speeds. In high winds the vertical velocity spectrum is somewhat steeper at high octaves and appears to flatten out more gradually at lower octaves than the spectra found in weak mean wind conditions.

Interestingly, none of the other spectra differ signif-

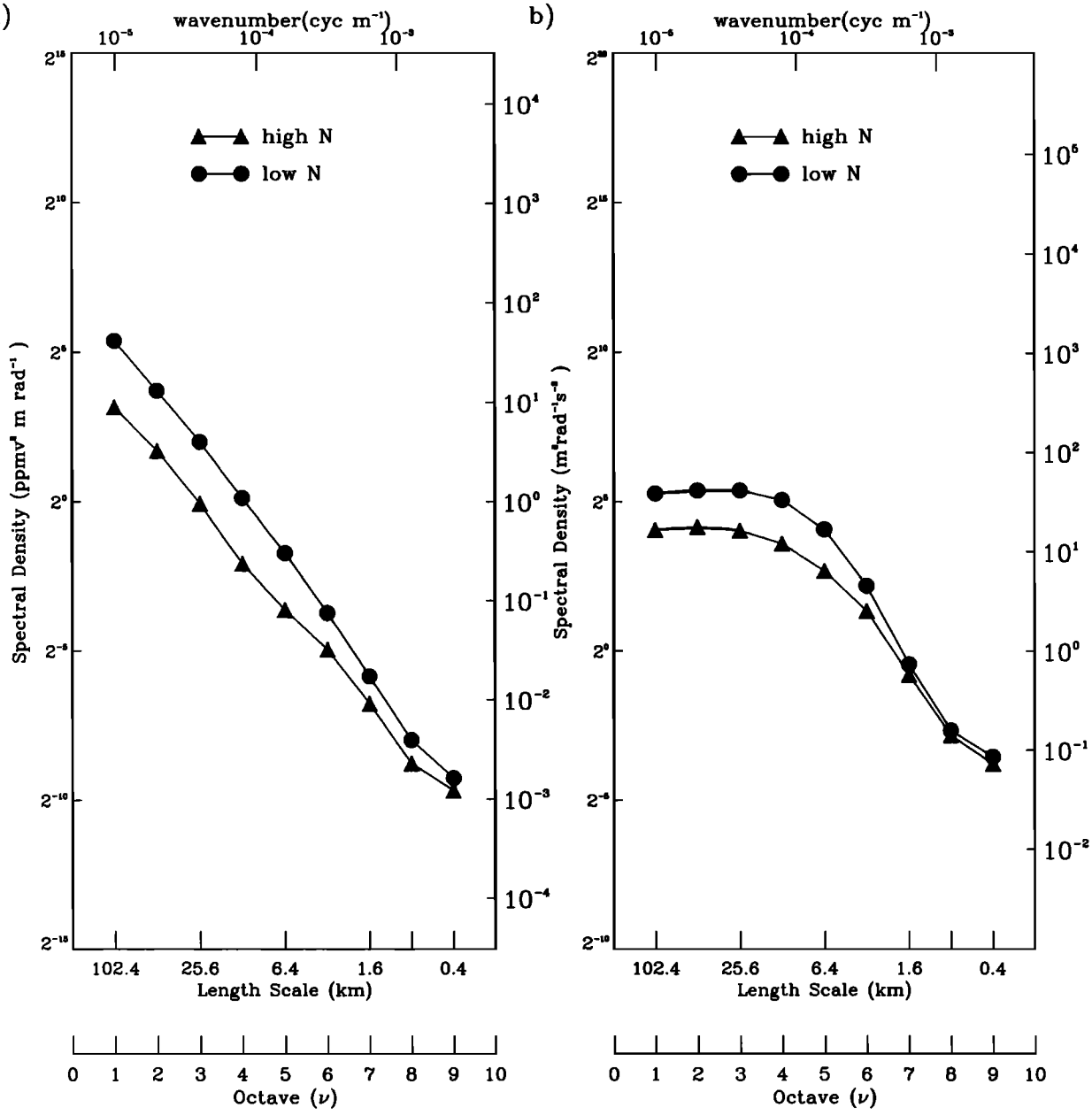

Figure 10. Log-averaged DWT power spectra of (a) ozone variance and (b) vertical velocity sorted according to magnitude of buoyancy frequency N. Two subsets of the data are constructed: one subset for measurements taken where $N > 0.023$ rad s^{-1} according to the NMC analysis and one where $N < 0.020$ rad s^{-1}. The high stratification group is denoted by the solid triangles, and the low stratification group is denoted by the solid circles.

icantly when sorted by mean horizontal velocity. The high-mean velocity and low-mean velocity power spectra for horizontal velocity, potential temperature and ozone are nearly indistinguishable from each other or from the set-averaged spectra. Figure 9a shows average spectra of zonal wind sorted according to mean velocity. For horizontal velocity and potential temperature both the shapes and the magnitudes of the high-mean and low-mean velocity spectra are the same. For ozone there is a small increase in variance at all horizontal scales for the high-mean velocity spectra. However, the shapes of the average ozone spectra for high-mean and low-mean velocity conditions are nearly identical.

This result is somewhat at odds with the findings of *Nastrom et al.* [1987], who obtained horizontal velocity spectra with slopes steeper than −5/3 primarily over rough terrain in high winds. In contrast, we see little difference in spectral slope between high- and low-wind environments. Our mean horizontal velocity spectra under all conditions are closer to the high-topography, high-wind spectra of *Nastrom et al.* [1987] than to the GASP climatological spectra. Although we have not isolated the oceanic segments in our data, we are confident that they would yield spectra very close to the set-average spectra in Figure 4. We make this inference because the slope histograms in Figure 6 are sharply

peaked despite the variety of geographical and meteorological environments encountered during AASE II, SPADE, and ASHOE/MAESA. In addition, over half of the total flight time during the three missions occurred over ocean. Thus we conclude that typical conditions in the midstratosphere are closer to conditions of enhanced variability in the GASP data than to climatological upper tropospheric and lower-stratospheric conditions as determined from the GASP data.

Effect of background Brunt-Väisälä frequency

Figure 10 shows the effects of varying values of the inferred background Brunt-Väisälä frequency N on the power spectra of ozone and vertical velocity. The values of N used to sort the spectra were derived from NMC analyses. This was done to increase the number of days over which N values were available from a single source. The MTP was not included on most of the SPADE flights due to payload weight considerations. However, intercomparisons of MTP-measured lapse rates and interpolated NMC lapse rates for AASE II and ASHOE/MAESA show generally adequate agreement for 1024-s average values. Nevertheless, this introduces a further source of uncertainty into the analysis.

The spectra were once again divided into two groups. One group consisted of spectra measured in environments with Brunt-Väisälä frequencies $N > 0.023$ rad s^{-1} and another of spectra measured where $N < 0.020$ rad s^{-1}. The most striking changes associated with stratification occur for the ozone power spectra in Figure 10a. Mean variance for the high-stratification group is reduced by nearly one decade at longer scales. At shorter scales the difference in variance between the high- and low-stratification groups is reduced. This implies a shallower ozone spectrum in highly stratified environments. Power spectra of horizontal velocity and potential temperature (not shown) exhibit only minor sensitivity to stratification.

The power spectra of vertical velocity (Figure 10b) show differences similar to those seen in Figure 9b. The power spectrum of vertical velocity in strongly stratified environments is similar to that in environments of low mean wind speed . The likely explanation for this lies in the distribution of NMC stratification frequencies associated with these missions. The histogram of N for the whole data set (Figure 11) shows a distinct double-peaked structure, with a large peak at $N \approx 0.02$ rad s^{-1} and a smaller secondary peak at $N \approx 0.025$ rad s^{-1}. The existence of two distinct peaks reflects the relatively sharp border between tropical and midlatitude conditions above the subtropical jet. NMC Brunt-Väisälä frequencies higher than 0.023 rad s^{-1} occur exclusively on tropical or equatorward flights. The relative sizes of the peaks simply reflect the higher number of mid-latitude and poleward flights during these missions. Tropical conditions tend to be associated with both weak horizontal wind speeds and high stratification. Thus there is a large overlap between the groups of data intervals containing weak mean horizontal wind speeds and those containing strong mean stratification. The major exceptions to this are the SPADE measurements, and the October 1991 to March 1992 deployments during AASE II. These data contain a high number of intervals with both light horizontal winds and low Brunt-Väisälä frequencies.

To isolate the effect of stratification on the power spectra of vertical velocity we discard intervals with mean horizontal wind speeds greater than 20 m s^{-1} before grouping by stratification. This reduces the indirect effects of mean horizontal velocity on our grouping by stratification. When this is done the differences

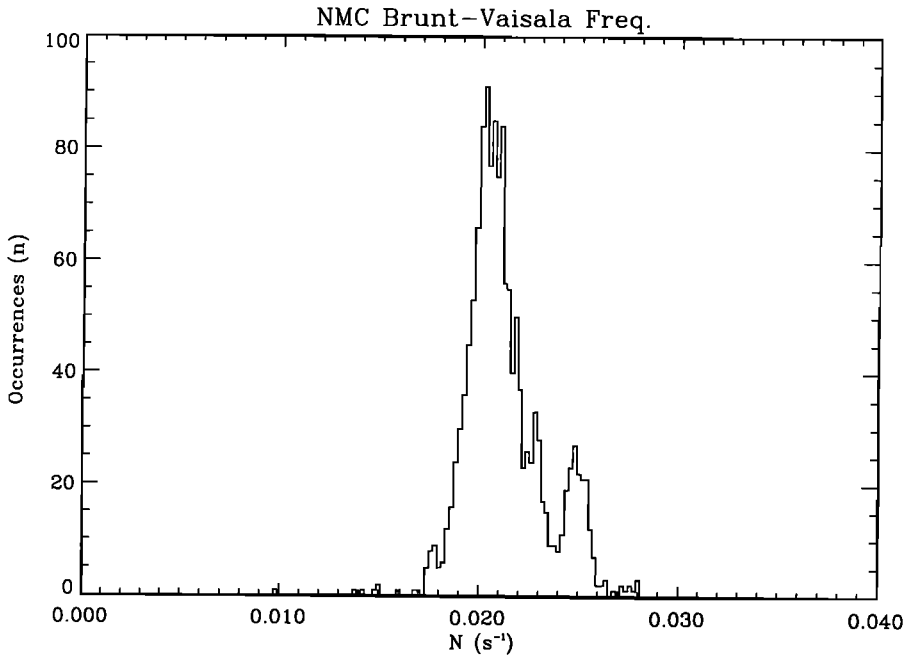

Figure 11. Histogram showing distribution of stratification frequency values N determined from NMC analyses for the entire data set. The secondary peak of high N values is almost exclusively asscociated with low-latitude or tropical flight segments.

seen between the high stratification and low stratification in Figure 10b disappear. Thus our velocity spectra do not appear to vary significantly with mean stratification, as was inferred in earlier high–wavenumber spectral studies of *Koprov*, [1965]; *Vinnichenko et al.*, [1965]; *Myrup*, [1968]; and *Shur*, [1971] and, more recently, in the analysis of GASP spectra [*Nastrom et al.*, 1987]. This may be the result of the limited range of Brunt-Väisälä frequencies in our data. Almost all of our data were taken in environments with $0.020 \text{ rad s}^{-1} \lesssim N \lesssim 0.025 \text{ rad s}^{-1}$. Thus the full range of the sampled N values may span $\lesssim$20% of the mean. The apparent sensitivity of the ozone spectra to N may reflect the difference between tropical and midlatitude-polar environments.

4. Taylor's Hypothesis in the Presence of Gravity Waves and Turbulence

4.1 Theory

Traditionally, aircraft spectra such as those used in this study have been derived by implicitly assuming Taylor's hypothesis, so that time variations measured by the aircraft can be converted to horizontal length scales by simply scaling the former by the aircraft's flight speed to obtain the latter. This requires that the time variations of the motions themselves are not significant, or that the aircraft spans their horizontal extent sufficiently fast that they do not vary temporally. Consequently, aircraft spectra are usually plotted as a function of horizontal wavenumber, as given by a Taylor transformation of time variations measured within the aircraft's frame of reference.

Here we interpret the aircraft data initially as frequency spectra measured from the aircraft's frame. This allows us to assess more accurately how gravity waves might influence these spectra, by treating them as frequency spectra which have been Doppler shifted from the intrinsic (atmosphere–based) frame to the aircraft frame. The theory of Doppler–shifted gravity wave spectra has been developed through efforts to reconcile ground-based measurements of velocity frequency spectra with the estimates of both gravity wave and 2-D turbulence theories, which are typically formulated in terms of intrinsic frequency [*Scheffler and Liu*, 1986; *Fritts and VanZandt*, 1987; *Vincent and Eckermann*, 1990; *VanZandt et al.*, 1991; *Gardner et al.*, 1993b]. The 2-D turbulence theories always adopt Taylor's hypothesis since this structure is taken to be "frozen" into the background flow. On the other hand, spectra produced by gravity waves will generally include contributions from motions which are propagating with respect to the background flow. If these propagation speeds are comparable to the observing frame speed, then a Taylor transformation will not recover the true horizontal wavenumber spectrum.

A general method for calculating Doppler–shifted gravity–wave spectra was given by *Scheffler and Liu* [1986], while *Fritts and VanZandt* [1987] presented more illustrative analytical solutions which incorporated many simplifications but retained the major effects. *Gardner et al.* [1993b] furthered this analytical approach by using updated versions of the intrinsic gravity-wave spectrum and by assuming isotropic horizontal propagation, rather than the one–dimensional (1-D) horizontal propagation considered by Fritts and VanZandt. We adopt the Doppler-shifting model of *Gardner et al.* [1993b] in our prediction of gravity wave frequency spectra as measured on the aircraft. Although their analytical model assumes a hydrostatic dispersion relation, their results differed little when compared with more complete numerical calculations which used a more accurate dispersion relation.

Gardner et al. [1993a,b] assumed separability of the 2-D intrinsic-frequency and vertical wavenumber spectrum of horizontal velocities produced by gravity waves, so that

$$E_{uv}(m,\omega) = u_{\text{tot}}^2 A(m) B(\omega),$$

where u_{tot}^2 is the total horizontal-velocity variance. *Gardner et al.* [1993a] used a piecewise-continuous model for the vertical wavenumber spectrum $A(m)$, shown with dashed lines in Figure 12a, whereas *Gardner et al.* [1993b] used an analytical model shown with the solid curve in Figure 12a. Both studies assumed $B(\omega) \propto \omega^{-2}$, as shown in Figure 12b. Similar models to these have been used in recent spectral parameterizations of gravity wave processes [*Fritts and VanZandt*, 1993] and agree broadly with spectral measurements of stratospheric gravity waves [*Fritts and Chou*, 1987; *Allen and Vincent*, 1995] .

Gardner et al. [1993a] used standard Jacobian transformations to derive the 1-D horizontal wavenumber spectrum $G_{uv}(k)$, assuming a hydrostatic dispersion relation and isotropic horizontal propagation directions. Their result is shown with the dashed curve in Figure 12c. Applying the hydrostatic polarization relations to the horizontal velocity spectrum yields the corresponding vertical velocity spectrum, i.e., $E_w(m,\omega) = \omega^2 N^{-2} E_{uv}(m,\omega)$. Using the transformations of *Gardner et al.* [1993a] we derive the 1-D horizontal wavenumber spectrum $G_w(k)$ for vertical velocity. This is shown with the dashed line in Figure 12d. We also derive models for $G_{uv}(k)$ and the corresponding vertical velocity spectrum $G_w(k)$ using the models for $A(m)$ and $B(\omega)$ adopted by *Gardner et al.* [1993b]. These are plotted with solid curves in Figs. 12c and 12d. The typical range of k values resolved in these aircraft data is shaded.

Note that the model horizontal wavenumber spectra do not depend greatly on the precise model used for $A(m)$. The *Gardner et al.* [1993a] model for $A(m)$ assumes $m^{-5/3}$ spectra beyond m_b, which is taken to represent the onset of inertial range 3-D turbulence. This also yields $k^{-5/3}$ spectra for $k \geq m_b$, as shown in Figure 12c and 12d, but of course gravity wave theory was not used to derive this result. The so-called buoyancy wavenumber $m_b \approx 2\pi/L_B$ is discussed in more depth below. It is also worth noting that the choice of

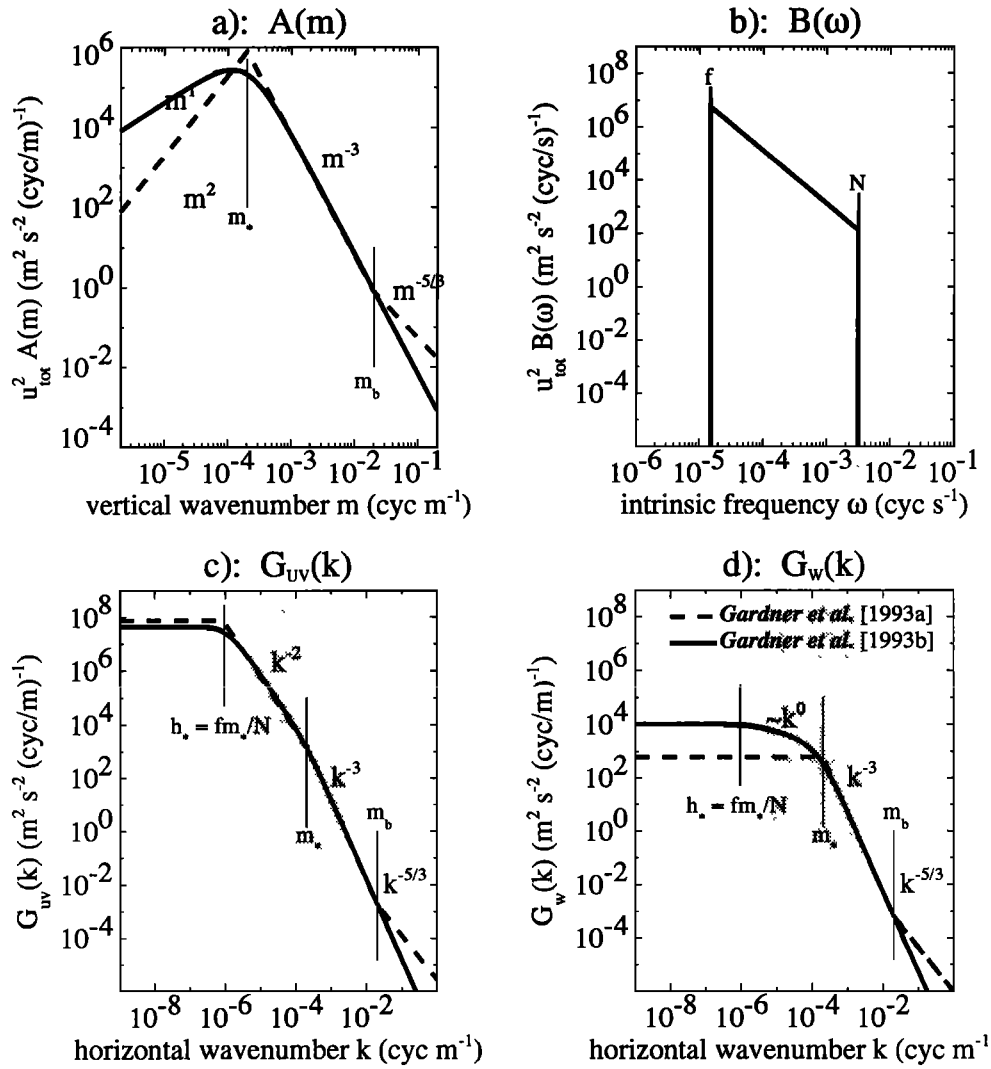

Figure 12. Power spectra of horizontal velocity. (a) Power in horizontal velocity as a function of vertical wavenumber m. Power peaks near vertical wavenumber m_*. Power laws for spectrum away from m_* are indicated on the figure. b) Power in horizontal velocity as a function of intrinsic (atmosphere based) frequency ω. Power is assumed to be zero for $\omega < f$, where f is the local rotation frequency, and for $\omega > N$, where N is the local Brunt-Väisälä frequency. Between f and N, power varies as ω^{-2}. (c and d) Doppler-shifted, Taylor-transformed power spectra for (c) horizontal, and (d) vertical velocities as a function of horizontal wavenumber. Shaded strip indicates scale range covered in this study. The amplitudes of the model spectra of horizontal velocity are chosen arbitrarily in this study.

the model intrinsic–frequency spectrum is directly reflected in the horizontal wavenumber spectrum for horizontal and vertical velocity for $h_* \ll k \ll m_*$, where we have $G_{uv}(k) \propto k^{-2}$. Other choices for the exponent in the intrinsic frequency spectrum would change the resulting horizontal wavenumber spectrum as well. In other words $B(\omega) \propto \omega^{-\alpha}$ will yield $G_{uv}(k) \propto k^{-\alpha}$ and $G_w(k) \propto k^{-\alpha+2}$ for $h_* \ll k \ll m_*$ for any choice of α. The k^{-3} behavior predicted for $k > m_*$ in both horizontal and vertical velocity power spectra results from the cutoff of wave energy at $\omega = N$ and the m^{-3} behavior assumed for energy at $m > m_*$ [*Gardner et al.*, 1993a].

Following *Fritts and VanZandt* [1987], *Gardner et al.* [1993b] found that their Doppler–shifted frequency spectra were conveniently characterized in terms of a Doppler–shifting parameter

$$\beta = \frac{m_*(\bar{U} - V\cos\phi)}{N}, \tag{4}$$

where $\bar{U}$ is the background wind speed, V is the aircraft's speed, and ϕ is the azimuth angle between the wind and aircraft velocity vectors. The parameter m_* is the vertical wavenumber at or near which the horizontal velocity power spectrum peaks (see Figure 12a), and is generally predictable and/or measurable (and relatively constant) at a given altitude [*Hines*, 1991; *Fritts and VanZandt*, 1993; *Allen and Vincent*, 1995]. Thus the strength of the effects depends mainly on the veloc-

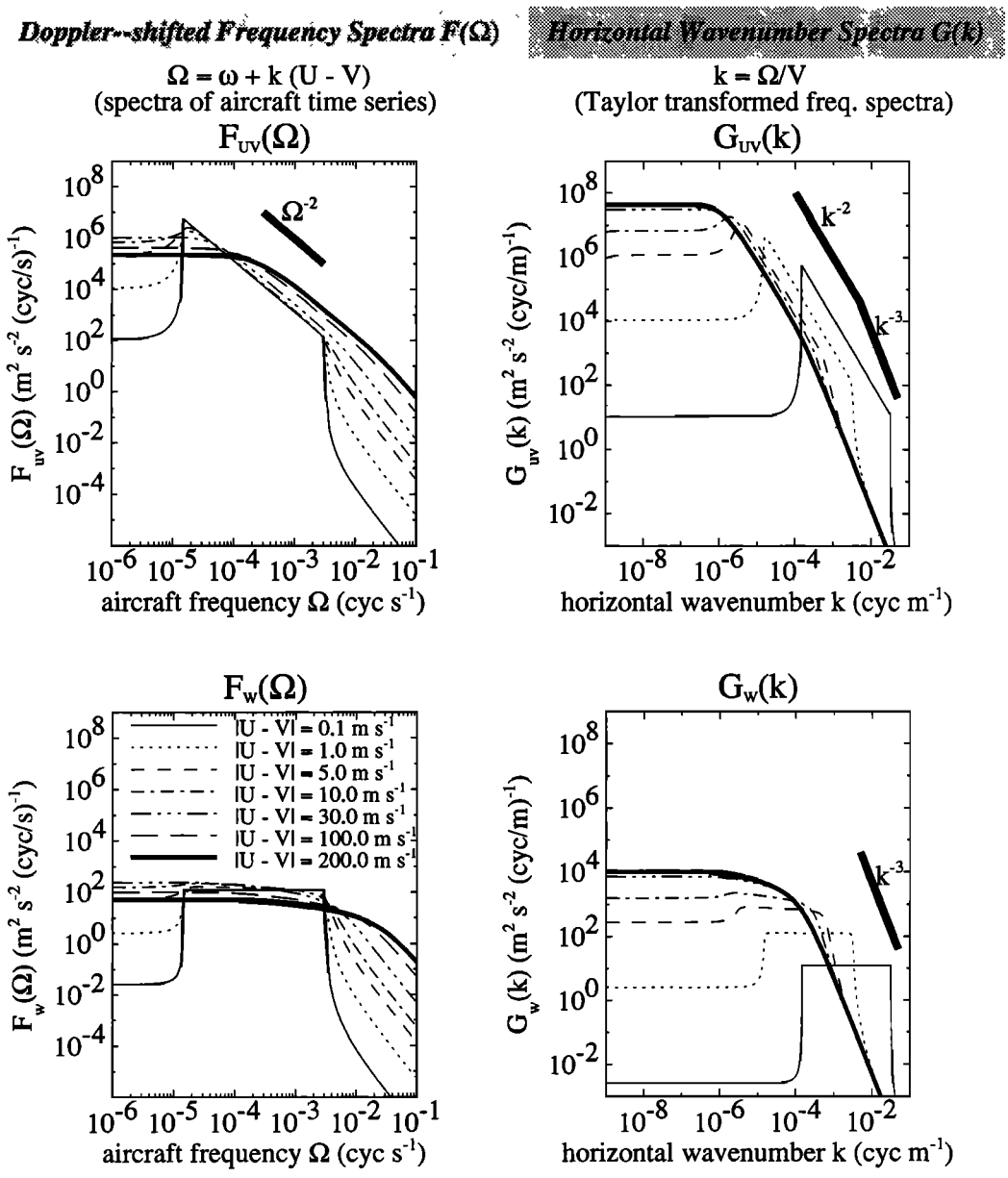

Figure 13. Theoretically derived horizontal wavenumber spectra for horizontal and vertical velocities. Left panels show frequency spectra of horizontal velocity (top left) and vertical velocity (bottom left) which would be measured in aircraft traveling at different speeds with respect to the atmosphere. Thin solid line shows spectra for airspeed of 0.1 m s^{-1} and should therefore be close to the unshifted or intrinsic frequency spectra shown in Figure 15. As relative airspeed increases, Doppler spreading smooths out the spectra. For airspeeds above 100 m s^{-1} (long dashes and thick solid line), the airplane speed exceeds the propagation speed of a greater and greater fraction of the wave energy in the assumed spectrum. Doppler spreading ceases to affect the shape of the measured spectra in a significant way. Right panels show airplane measured frequency spectra transformed to horizontal wavenumber spectra using a Taylor transformation. Parameters for assumed gravity spectrum are $N = 0.02$ rad s^{-1} and $m_* = 2\pi/(3$ km). A value of f correpsonding to a latitude of 40° is used.

ity difference in (4). One should note that *Fritts and VanZandt* [1987] and *Gardner et al.* [1993b] considered ground-based frames exclusively, and so the frame speed term $V\cos\phi$ does not appear in their analysis since it is always zero.

To simplify the discussion as much as possible, we shall consider the aircraft and wind velocities to be parallel along an east–west axis, since $\bar{U}$ is generally zonal. By allowing the speeds $\bar{U}$ and V to become positive or negative zonal velocities, then (4) can be simplified to yield

$$\beta = \frac{m_*(\bar{U} - V)}{N}. \tag{5}$$

Note that when $\bar{U} = V$, $\beta = 0$ and no Doppler shifting occurs, as expected.

The left panels of Figure 13 show the frequency spectra of horizontal velocities, $F_{uv}(\Omega)$ (top), and vertical velocities, $F_w(\Omega)$ (bottom), as measured on an aircraft moving at seven different speeds with respect to the background wind, $|\bar{U} - V|$ [*Gardner et al.*, 1993b]. We choose $m_* = 2\pi(3\text{ km})^{-1}$ and $N = 0.02$ rad s^{-1}, as they are typical values in the lower stratosphere [*Fritts and Chou*, 1987; *Tsuda et al.*, 1991; *Allen and Vincent*, 1995] see also Figure 11. Note the different frequency spectral shapes that occur in all seven cases. We have computed these model spectra by assuming equal amounts of wave energy propagating in all horizontal directions in the intrinsic frame. This is often a good approximation, since the accumulative effect of critical levels in filtering wave propagation directions is usually limited in the lower stratosphere (although not always [see *Eckermann*, 1995]). The ultimate Taylor transformation to a horizontal wavenumber spectrum, however, proves relatively insensitive to these details.

The corresponding panels on the right of Figure 13 show the result of applying a Taylor transformation to the aircraft frequency spectra on the left, whereupon horizontal wavenumbers k are given by $k = \Omega/V$, and the horizontal wavenumber spectrum is given by [e.g., *Vincent and Eckermann*, 1990]

$$G_{uv}(k) = F_{uv}(kV)\ V, \tag{6}$$

and likewise in transforming from $F_w(\Omega)$ to $G_w(k)$. If we assume that the variability in potential temperature θ' and trace gas mixing ratios χ' is due to vertical gravity wave displacements ζ' acting on a mean vertical distribution of potential temperature $\overline{\Theta}(z)$ or mixing ratio $\overline{\chi}(z)$, i.e.,

$$\chi' = \zeta'\frac{\partial}{\partial z}\overline{\chi}(z) \qquad \theta' = \zeta'\frac{\partial}{\partial z}\overline{\Theta}(z),$$

then, using the hydrostatic polarization relations we can derive transformed variance spectra for potential temperature, ozone and N_2O. Using $|\zeta'| = |(u', v')|/N$, these become

$$G_\theta(k) = \left(\frac{1}{N}\frac{\partial}{\partial z}\overline{\Theta}\right)^2 G_{uv}(k)$$

for potential temperature, and

$$G_\chi(k) = \left(\frac{1}{N}\frac{\partial}{\partial z}\overline{\chi}\right)^2 G_{uv}(k)$$

for ozone or N_2O. Thus linear gravity wave theory predicts the same spectral shape for potential temperature and ozone or N_2O variance as it does for horizontal velocity variance.

We note from Figure 13 that when $|\bar{U} - V| \gtrsim 30$ m s^{-1} ($\beta \gtrsim 3$), the frequency spectra Taylor–transform to overlying wavenumber spectra which are identical to the model spectra in Figs. 12c and 12d. This indicates that, in these cases, the Taylor transformation is valid and recovers the true gravity wave horizontal wavenumber spectrum. However, when $|\bar{U} - V| \lesssim 30$ m s^{-1} ($\beta \lesssim 3$), the inferred horizontal wavenumber spectra in Figure 13 differ in shape. In these cases, Taylor's hypothesis is invalid, since the temporal oscillations of the waves themselves are significant and contaminate the inversion. These analytical results confirm, via a somewhat different but essentially equivalent route, the numerical simulations of *Gardner and Gardner* [1993]. Assuming $\bar{U} = 0$, they concluded that aircraft–derived horizontal wavenumber spectra produced by lower–stratospheric gravity waves would not be distorted significantly when $|V| \gg 6$ m s^{-1} ($\beta \gg 1$).

Fortunately $|V| \approx 200$ m s^{-1} in these aircraft experiments, which usually ensures $|\bar{U} - V\cos\phi| \gtrsim 50$ m s^{-1} when one takes into account mean winds and the $\cos\phi$ effects. Hence Taylor's hypothesis appears valid for any gravity waves in the data. Since the Taylor hypothesis is always valid for 2-D turbulence, and should also hold for inertial and buoyancy–modified 3-D turbulence at these large aircraft speeds [e.g, *Powell and Elderkin*, 1974; *Wyngaard and Clifford*, 1977], then a Taylor transformation to infer wavenumber spectra can be applied fairly confidently to these aircraft data, regardless of their dynamical content.

4.2 Comparison With Aircraft Velocity Spectra

The Taylor–transformed spectra on the right of Figure 13 faithfully reproduce the model horizontal wavenumber spectrum of gravity waves when $|U - V|$ is large. On inspecting these curves we note that, at intermediate horizontal scales, $F_{uv}(k)$ varies as k^{-2}, while $F_w(k)$ is essentially flat. At larger k both spectra exhibit a break towards k^{-3} shapes. This break occurs at $k = m_*$ in Figure 13 [e.g., *Gardner et al.*, 1993a] or at an approximate Fourier scale of $2\pi 5$ km, assuming a typical range of stratospheric m_* values. A direct comparison of theoretically derived aircraft velocity spectra with the observed aircraft spectra is shown in Figure 14. The most significant result is the successful prediction of the horizontal scale at which the spectral index changes value, that is, at a horizontal scale corresponding to $k = m_*$. As discussed in section 4.1, this break in the horizontal wavenumber spectra is a direct consequence of the cutoff in wave energy at $\omega = N$, which was assumed in the model intrinsic frequency spectrum. The location of the spectral break at a given horizontal scale is determined by the choice

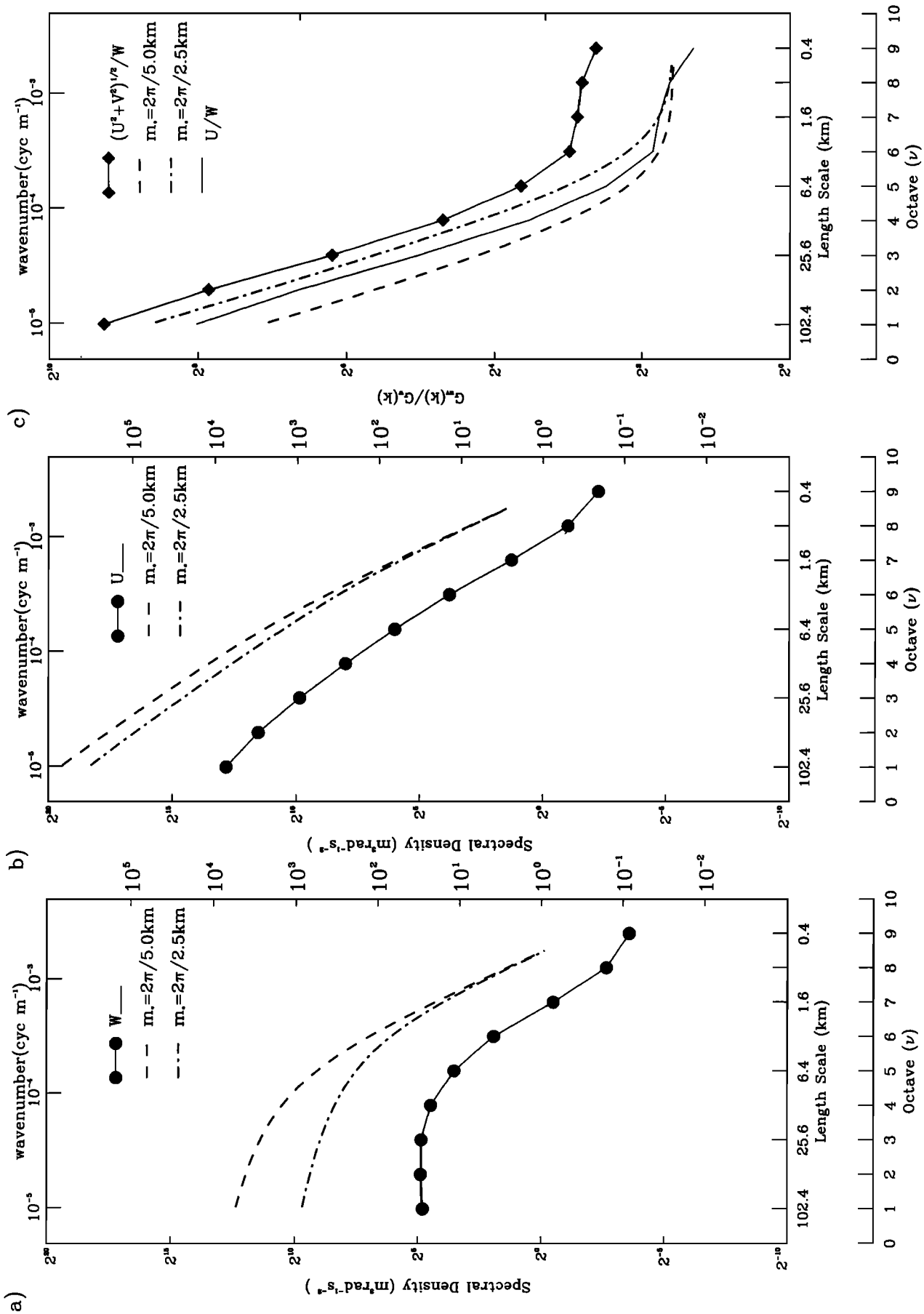
a)
b)
c)
Spectral Density (m²rad⁻¹s⁻²)
wavenumber(cyc m⁻¹)
Length Scale (km)
Octave (ν)
W
U
m.=2π/5.0km
m.=2π/2.5km
(U²+V²)^1/2/W
U/W
G_uu(k)/G_vv(k)

of m_* in the model spectrum. However, balloon and profiler data consistently indicate values of m_* between $2\pi(2\text{ km})^{-1}$ and $2\pi(5\text{ km})^{-1}$ for the lower stratosphere [e.g, *Fritts and Chou,* 1987; *Tsuda et al.,* 1991; *Allen and Vincent,* 1995]. This range of m_* values leads to breaks in the model horizontal wavenumber spectra, which are in good agreement with those observed in the ER-2 data.

The values of the spectral indices within each regime are also well predicted by the model spectra. For high wavenumbers, $k > m_*$, the observed spectra behave as $k^{-2.5}$, which is close to the k^{-3} behavior predicted by the model gravity wave spectra. The high wavenumber k^{-3} behavior in the model spectra is related to the high wavenumber m^{-3} tail in the assumed vertical wavenumber spectrum $A(m)$, which is well established from observations. For smaller horizontal wavenumbers the observed and predicted spectra are also in good agreement. However, at these longer scales the spectral index of the model velocity spectra is directly related to the assumed shape of intrinsic frequency spectrum $B(\omega)$, which must be inferred from measurements of ground-based frequency. It may also be worth noting that the differences between the theoretical vertical velocity spectra for $m_* = 2\pi(2.5\text{ km})^{-1}$ and $m_* = 2\pi(5\text{ km})^{-1}$ in Figure 14 are reminiscent of the differences between the average vertical velocity spectra for conditions of strong horizontal velocity and those of weak horizontal velocity in Figure 9b.

In this study, we regard the amplitude of the initial model spectrum of horizontal velocity $E_{uv}(\omega, m)$ as arbitrary. However, the linear polarization relations for gravity waves still determine the amplitude of the vertical velocity spectrum once an amplitude for the horizontal velocity spectrum has been chosen. Thus the gravity wave theory specifies the ratio of horizontal velocity variance to variance of vertical velocity as a function of horizontal wavenumber. Figure 14c compares theoretical predictions of $G_{uv}(k)/G_w(k)$ with measured ratios of horizontal and vertical velocity power spectral densities. The solid diamonds show the observed ratio of the spectral density of total horizontal velocity to that of vertical velocity. As in section 3.3, the spectral density of total horizontal velocity is the sum of the zonal and meridional components (Figure 4a) at each octave. The thin line in Figure 14c shows the ratio of the spectral density of zonal velocity variance to that of vertical velocity. However, assuming an isotropic gravity wave spectrum, the appropriate comparison between our theory and observations is with the ratio of total horizontal velocity to vertical velocity. The theory predicts a ratio approaching 3.0 for horizontal wave numbers $k > m_*$, and predicts rapidly increasing ratios at lower wavenumbers. In general, the theoretical ratio at $k > m_*$ approaches $(5-p)/(3-p)$ for $B(\omega) \propto \omega^{-p}$. The observed ratio of the set-averaged horizontal velocity spectra agrees reasonably well with the prediction of the gravity wave theory at longer scales. The agreement between observations and theory seems to be somewhat better for $m_* = 2\pi(2.5\text{ km})^{-1}$, although an even larger value of m_* may be indicated by the data. At smaller scales (<6 km) the theoretical ratio begins to deviate significantly from the observed ratio. The theoretical ratios approach a value of 3.0 for scales less than $2\pi/m_*$, while the observed ratios are close to 6. Although discrepancies occur at shorter scales, the general shape of the observed ratio curve is close to the theoretical prediction. Overall, the agreement obtained here between the theoretical and observed horizontal-to-vertical velocity ratio is much closer than that in previous studies [e.g., *Gage et al.,* 1986]. In their analysis of radar data, *Gage et al.* [1986] report differences of up to 2 orders of magnitude between the observed ratio of horizontal to vertical velocity and that predicted by a gravity wave theory.

Several explanations are possible for the discrepancy between observed and theoretical velocity ratios in this study. First, the theoretical ratio $G_{uv}(k)/G_w(k)$ in the high–wavenumber k^{-3} tail is somewhat sensitive to the assumed shape of $B(\omega)$. Steeper $B(\omega)$ will lead to larger $G_{uv}(k)/G_w(k)$ in the tail portion of the spectrum. However, there is no evidence for $B(\omega)$ steeper than the -2 power law assumed here. Second, if there are preferred directions of propagation, then the total horizontal velocity variance may be closer to either the individual meridional or zonal velocity variances, which would lead to lower observed horizontal-to-vertical velocity ratios at high k. This is evident in the observed zonal to vertical velocity ratio shown in Figure 14c. Finally, it is possible and quite likely that our gravity wave theory is incomplete at short horizontal scales. Gravity waves at these scales are likely to be near saturation as well as being nonhydrostatic.

The possibility that quasi-2-D turbulent motions are

Figure 14. Comparison of measured log-averaged DWT horizontal wavenumber spectra of zonal and vertical velocity (from Figures 4b and 6b respectively) with theoretical predictions for spectra measured by an airplane travelling at 200 m s^{-1}. (a) Comparison for vertical velocity. Short-long dashed curve shows prediction for $m_* = 2\pi/(2.5\text{ km})$. Long dashes show prediction for $m_* = 2\pi/(5\text{ km})$. (b) Same as Figure 14a except for zonal wind. It should again be noted that the amplitude of the model spectra is arbitrary. (c) Ratio of horizontal velocity variance to vertical velocity variance as a function of horizontal wavenumber. Solid diamonds show measured ratio obtained from set-averaged DWT power spectra of total horizontal velocity and vertical velocity. Solid curve shows observed ratio of zonal velocity to vertical velocity. Short-long dashed curve shows theoretically predicted variance ratio for $m_* = 2\pi/(2.5\text{ km})$ as a function of horizontal wave number. Long dashed curve shows prediction for $m_* = 2\pi/(5\text{ km})$.

responsible for the apparent excess of horizontal kinetic energy cannot be discounted [*Gage et al.*, 1986]. However, if this is the case then it must be explained why the excess appears most pronounced at scales shorter than 6 km, and why little excess of horizontal kinetic energy is apparent at scales longer than 6 km. It is curious that the observed horizontal-to-vertical velocity ratio and the theoretical ratio differ by a fairly uniform factor of 2 at short scales. This means that any excess horizontal kinetic energy must also have a k^{-3} spectrum at small scales, whatever its dynamical origin. Furthermore, this excess horizontal energy must also break to a shallower spectrum at around $k = m_*$. Otherwise, it would quickly dominate the observed horizontal velocity spectrum, which has a $k^{-1.5}$ to k^{-2} at scales longer than $k = m_*$.

Our measured velocity wavenumber spectra at large k are very similar to those derived from high-resolution tropospheric and lower stratospheric measurements over 30 years ago by *Shur* [1962], and later by *Vinnichenko et al.* [1965], *Koprov* [1965], *Myrup* [1968], *Shur* [1971], *Lilly and Lester* [1974], and *Berman* [1976]. In each of these studies, horizontal wavenumber spectra of velocity with spectral indices more negative than −5/3 were obtained. These observations were clearly inconsistent with the onset of inertial-range 3-D turbulence. It was through efforts to explain these anomalous data that the Lumley–Shur theory of a buoyancy-modified subrange of turbulence first arose [*Shur*, 1962; *Bolgiano*, 1962; *Lumley*, 1964]. This theory was subsequently refined in several later studies [e.g., *Weinstock*, 1978, 1985b] and has sometimes been invoked as a possible explanation of m^{-3} horizontal velocity spectra observed at larger vertical wavenumbers m [e.g., *Weinstock*, 1985a; *Sidi and Dalaudier*, 1989], a spectral region more traditionally ascribed to interacting and/or dissipating gravity waves [e.g., *Smith et al.*, 1987; *Weinstock*, 1990; *Hines*, 1991; *Gardner*, 1994; *Zhu*, 1994]. In fact, *Lumley* [1964] argued that his buoyancy-subrange theory was applicable regardless of whether the motions were gravity waves or turbulence.

A buoyant-subrange velocity spectrum sets in at wavenumbers smaller than the buoyancy wavenumber $k_B = 2\pi/L_B$, given by

$$L_B = \frac{2\pi}{\tilde{C}} L_0, \tag{7}$$

$$L_0 = \left(\frac{\epsilon}{N^3}\right)^{1/2}, \tag{8}$$

where ϵ is the energy dissipation rate, $\tilde{C}$ is some scaling constant, and L_0 is the so-called Ozdimov scale. The scaling constant $\tilde{C}$ was not determined by *Lumley* [1964]. *Weinstock* [1978] developed the buoyant-subrange theory further, predicting kinetic energy spectra $\sim k^p$, where $-4/3 < p < -2.5$ at scales between L_B and $10L_B$. He also derived a value $\tilde{C} = C(u_m/u_0)^{-3/2}$, where $C \approx 0.62$, u_0 is the rms velocity within the inertial subrange, and u_m is the rms velocity over the entire spectrum from the scale of the energy source to $k = \infty$. *Weinstock* [1978] suggested $u_m/u_0 \lesssim 3$ ($L_B \lesssim 50 L_0$) for weak decaying turbulence. However, based on subsequent atmospheric, oceanic and laboratory studies which indicated that these L_B/L_0 ratios were too large, *Weinstock* [1992] derived a new relation $\tilde{C} = (0.16 Ri_0)^{-3/4}$, where Ri_0 is the turbulent gradient Richardson number. Using stratospheric values for N, and given the possible wide variations in ϵ, u_m/u_0 and Ri_0 (and hence $\tilde{C}$), (7)–(8) yields a range of values for the buoyancy scale $L_B \sim 10 - 300$ m in the stratosphere [e.g., *Weinstock*, 1985a; *Hocking*, 1985]. This would be consistent with our observed spectral indices of approximately −2.5 for both horizontal and vertical velocity at scales below 3.2 km. Thus an ambiguity in interpretation exists at the high k range of our observations. The theory of buoyant subrange turbulence and gravity wave theory give similar results. However, this agreement may reflect a true ambiguity in the nature of the motion at these scales.

The shapes of the aircraft horizontal velocity spectra at $k \ll 2\pi/5$ km resemble those found in previous measurements in the troposphere and mesosphere, with spectral indices typically in the range −1.5 to −2 [e.g., *Nastrom and Gage*, 1985; *Nastrom et al.*, 1987; *Fritts et al.*, 1989; *Kwon et al.*, 1990; *Hostetler and Gardner*, 1994]. There are few published stratospheric measurements of this kind, however. Spectra derived from "HICAT" data were collated from various sources and reviewed inter alia by *Weinstock* [1978]. They apparently suggested spectra closer to $k^{-5/3}$ at larger scales. *Lilly and Lester* [1974] presented spectra of along-track Doppler wind velocities and potential temperature which suggested k^{-3} spectra at scales $\lesssim$10–20 km, although their data were inaccurate at scales $\lesssim$2 km. *Murphy* [1989] presented various ER-2 spectra but used them more to verify the accuracy of the measurements. *Hostetler and Gardner* [1994] presented spectra of relative density fluctuations but could not measure their spectral indices with any accuracy. None of these earlier experiments appear to have noted the break from spectra described by $k^{-1.5}$ or k^{-2} to steeper spectra described by k^{-3}. *Lilly and Lester* [1974] also presented a vertical velocity spectrum inferred from the potential temperature using gravity wave arguments, which forced the spectrum toward k^{-1} behavior at large k. Thus it appears that direct measurements of stratospheric vertical velocity spectra, as presented here, have not been reported previously.

Thus our observations tend to confirm the earliest tropospheric observations of horizontal wavenumber spectra, and agree less with later observations which claimed $k^{-5/3}$ behavior within the buoyancy subrange and at even larger scales [e.g., *Weinstock*, 1978; *Nastrom and Gage*, 1985]. The spectra appear to be consistent with gravity waves and, at larger scales, also with predictions of the Lumley–Shur–Weinstock theory of a buoyant subrange of turbulence and/or gravity waves.

The spectral transformations involved in producing Figures 13 and 14 assume that the gravity-wave dispersion relation holds everywhere [*Gardner et al.*, 1993ab].

The Doppler–spreading model of *Hines* [1991] argues that the dispersion relation is invalidly applied in transforming to the portion of the spectrum which yields the high wavenumber k^{-3} spectra in Figures 12-14, since strong wave–wave interactions make linear theory inapplicable here. However, *Hines* [1991] cited modeling of oceanic gravity wave spectra by *Allen and Joseph* [1989] in which a cutoff horizontal wavenumber k_c was postulated, beyond which dynamical nonlinearities yielded k^{-3} spectra for both horizontal and vertical velocities measured in any Eulerian frame. S. D. Eckermann and D. Broutman (manuscript in preparation, 1996) applied Hines' Doppler–spreading ideas to show that they predict a cutoff wavenumber $k_c \approx 2m_*$, and hence at a horizontal wavelength ~4–10 km, similar to what we observe here.

5. Discussion

5.1 Aircraft Spectra of Velocity and Potential Temperature

The good agreement between the theoretically predicted aircraft velocity spectra and the observed aircraft spectra shown in Figure 14 is a compelling argument for a gravity wave interpretation of the variablilty within the range of horizontal scales covered by our observations (100 km $\gtrsim \lambda \gtrsim$ 1 km). The shapes of our observed and theoretical spectra, in particular, those for vertical wind, contrast sharply with the predictions of a combined inverse-cascading, 2-D and inertial-range, 3-D turbulence theory, which would have $k^{-5/3}$ everywhere for $G_{uv}(k)$, and would yield a similarly–shaped spectrum for $G_w(k)$ whenever the aircraft flies nonparallel to surfaces of constant potential temperature [e.g., *Gage*, 1979; *Gage and Nastrom*, 1990]. It should also be emphasized that a downscale, 2-D enstrophy cascade characterized by a kinetic energy spectrum $\sim k^{-3}$ can coexist with our model wave spectrum without fundamentally affecting our interpretation of the results. The contribution of the 2-D turbulent motion to kinetic energy would be greatest for the horizontal component of kinetic energy. Therefore its presence would probably be reflected as an excess of horizontal kinetic energy over that which would be derived from the vertical component using a pure wave interpretation. However, the ratio of horizontal–to–vertical velocity variance in our data does not suggest the presence of large amounts horizontal kinetic energy which cannot be accounted for by the wave interpertration (Figure 14c). Thus, while an enstrophy cascade may be present in the stratosphere, its contribution to kinetic energy at scales less than 100 km appears to be small compared to that of gravity wave motions.

It seems reasonable to assume that a transition to a kinetic energy spectrum dominated by 2-D turbulence will occur at some wavenumber. Our theoretical spectrum of gravity waves (Figure 12), which is at least partially supported by observation, assumes a complete cutoff of gravity wave energy at an intrinsic frequency $\omega = f$. This results in a flat horizontal wavenumber spectrum for horizontal velocity at scales longer than $2\pi/h_*$, where $h_* = fm_*/N$, for the horizontal wavenumber spectra $G_{uv}(k)$ in Figures 13 and 14. In reality, gravity wave energy may drop off more gradually as ω approaches f, leading to a more gradual decrease in the slope of the horizontal velocity spectrum. In any case, the gravity wave interpretation predicts flattening of horizontal velocity spectrum at scales $\sim 2\pi/h_* \approx 1000$ km for typical stratospheric values of N and m_* and midlatitude values for f. Thus we would predict that somewhere near this scale, contributions to the energy spectrum from sources other than gravity waves would begin to overwhelm the gravity wave spectrum. Spectra obtained from GASP data show a transition from a horizontal velocity power spectrum following a $k^{-5/3}$ law to a spectrum $\sim k^{-3}$ at a horizontal scale near 1000 km [*Gage and Nastrom*, 1985]. *Gage and Nastrom* 1985 argue that this is the scale at which the inverse energy cascade from mesoscale energy injections encounters the downscale enstrophy cascade from synoptic–scale energy injections. An alternative explanation for the change in spectral slope is that the observed transition from $k^{-5/3}$ behavior to k^{-3} behavior at around 1000 km reflects a transition from a gravity–wave–dominated energy spectrum at smaller scales directly to one dominated by enstrophy–cascading 2-D turbulence energized by synoptic–scale inputs. Similar conclusions were arrived at by *Yuan and Hamilton* [1994] based on nonlinear numerical simulations using a shallow water model.

In the 2-D turbulence view, the location of the transition from the inverse energy cascade to the downscale enstrophy cascade must be related to the relative magnitudes of the synoptic–scale energy injections and the mesocale energy injections. As the mesoscale injection decreases in magnitude relative to the synoptic–scale injection, the transition from $k^{-5/3}$ to k^{-3} behavior would occur at higher wavenumbers or shorter spatial scales. Specifically, a one–decade decrease in the magnitude of mesoscale energy injections relative to synoptic–scale energy injections, should shift the transitional wavenumber up by 3/4 of a decade. It is unlikely that the relative magnitude of synoptic and mesoscale injections is the same at all heights in the atmosphere. In particular, inputs from small-scale and mesoscale convection should decrease rapidly with altitude above the tropopause. Thus it would seem improbable that pure, 2-D turbulence would produce transitions from $k^{-5/3}$ to k^{-3} behavior at the same scale for all altitudes. On the contrary, above the tropopause, we would expect the transition to occur at higher wavenumbers than in the troposphere. The theoretical gravity wave spectra shown in Figure 12 predict more wave energy at low horizontal wavenumbers as m_* and, consequently, h_* decrease. The peak vertical wavenumber m_* is observed to decrease with altitude, presumably because nonlinear effects become important for longer vertical scales as wave amplitudes grow with altitude [*Smith et al.*, 1987; *Hines*, 1991]. Thus the combined wave–enstrophy cas-

cade picture would predict transitions from $k^{-5/3}$ to k^{-3} behavior at lower horizontal wavenumbers (longer scales) for higher altitudes.

A possible counterargument to the above scenario would be that a probable scale for energy injection into the middle atmosphere exists at a horizontal scale of around 100 km. This source could be, for example, breaking mountain waves. Such a source would increase with altitude as more and more waves break. This energy could go either into a spectrum of secondary gravity waves or into the inverse-cascade regime of 2-D turbulence. This could still be consistent with a gravity wave interpretation of motion at scales much smaller than 100 km.

5.2 Aircraft Spectra of Atmospheric Tracers

The ozone and N_2O spectra in this study are exceptional in that they tended to conform to a $k^{-5/3}$ power law. Similar results have been inferred from most previous spectral studies of tracer–like chemicals at these horizontal scales [*Nastrom et al.*, 1986; *Gage and Nastrom*, 1986; *Tjemkes and Visser*, 1994] including earlier analyses of ER-2 trace gas measurements from AAOE and AASE [*Murphy*, 1989; *Strahan and Mahlman*, 1994]. The $k^{-5/3}$ behavior obtained for horizontal wavenumber spectra of trace gas mixing ratios has typically been attributed to the inverse energy cascade of 2-D turbulence [*Nastrom et al.*, 1986].

However, since our spectra of horizontal velocity and potential temperature do not conform to predictions for inverse-cascading 2-D turbulence, interpretation of the contemporaneous ozone spectra in terms of 2-D turbulence is made difficult. Studies employing high-resolution contour advection or other air-parcel advection techniques [e.g., *Schoeberl et al.*, 1993a,b; *Pierce et al.*, 1994 *Plumb et al.*, 1994; *Waugh et al.*, 1994; *Waugh and Plumb*, 1994] have shown that large-scale ($\lambda \sim 1000$ km) 2-D horizontal motions in the stratosphere rapidly produce highly distorted tracer distributions with large variability at much smaller scales ($\lambda < 100$ km) even when the initial tracer field was smooth. Furthermore, the existence of these "vortex filaments" can be confirmed through comparison of these high-resolution advective calculations with aircraft measurements of atmospheric trace species [*Schoeberl et al.*, 1993b; *Plumb et al.*, 1994; *Waugh et al.*, 1994] and with satellite measurements [*Pierce et al.*, 1994]. In each of these studies, the large-scale atmospheric horizontal velocity fields are obtained from global meteorological analyses (e.g., NMC/CAC). These relatively coarse velocity fields are used to advect large numbers of purely passive trace particles. Estimates of long-lived trace gas mixing ratios for each air parcel can be estimated, for example, by using the air parcel's initial potential vorticity and potential temperature in conjunction with large-scale zonally averaged reconstructions of mixing ratio [*Lait et al.*, 1990].

None of the studies cited above derived spectra for their calculated tracer distributions. However, the passive nature of the calculations makes upscale energy transfer impossible for scales smaller than the resolution limit of the meteorological analyses $\gtrsim 2.5° \times 2.5°$ (inverse energy cascading could be implicit in the analyses at larger scales). Overall, the geometry of these high-resolution advective calculations strongly resembles that in the final stages of fully nonlinear 2-D calculations by *McWilliams* [1984]. In these calculations a small number of isolated, coherent, "hard core" vortices emerge from random noise initial conditions. Between these coherent vortices the flow is charcterized by essentially passive advection of vorticity filaments. Strong shears distort and stretch the filaments, generating smaller and smaller scales (i. e. enstrophy cascading). Thus, it seems likely that tracer spectra derived from high-resolution, advective calculations in the stratosphere would be those associated with the downscale enstrophy cascade of 2-D turbulence. *Lesieur and Herring* [1985] have theoretically derived tracer variance spectra which vary as k^{-1} in this regime. The shallow slope of the tracer variance spectrum means that enstrophy-cascading, quasi-horizontal turbulence can play an important role in producing tracer variability, while at the same time contributing little to the velocity and potential temperature spectra. Therefore, even if the apparent excess of horizontal kinetic energy at small scales in Figure 14c does not represent quasi-horizontal turbulence, quasi-horizontal turbulence may still significantly perturb trace gas distributions in the lower stratosphere.

The success of parcel advection models in reproducing many of the small-scale ($\lambda < 100$ km) features observed in aircraft trace gas data [*Plumb et al.*, 1994; *Waugh et al.*, 1994] suggests that enstrophy-cascading 2-D turbulence is producing some of the variability included in our spectra. However, our average power spectra for ozone are clearly steeper than the k^{-1} derived for tracers within enstrophy-cascading 2-D turbulence by *Lesieur and Herring* [1985]. It is possible that chemical processes are modifying the spectrum of ozone. Expected lifetimes for ozone in the lower stratosphere typically range from several weeks to several months, but enhanced destruction of ozone may occur if heterogeneous chemical processing is present. This cannot be ruled out for flights near the southern hemipshere winter polar vortex. However, N_2O has a sufficiently long photochemical lifetime in the altitude range 12-20 km that any chemical source and sink effects on mesoscale variability can be safely excluded. Thus it appears unlikely that chemical processes play a key role in producing the observed horizontal wavenumber spectrum of ozone and N_2O.

We currently have no satisfactory explanation for the observed spectrum of ozone and N_2O mixing ratio variance in the ER-2 data. As stated earlier, the spectral indices for ozone and N_2O are consistent with the $k^{-5/3}$ spectra predicted for a tracer in the inverse energy cascade of 2-D turbulence [*Lesieur and Herring*, 1985; *Nastrom et al.*, 1986]. However, two arguments against this interpretation have already been implied and are reiterated explicitly here: (1) the existence of the average

horizontal velocity and potential temperature spectra with indices clearly more negative than −5/3 at scales for which a spectral index of −5/3 is obtained for ozone and N_2O; and (2) the success achieved by other investigators in reproducing small-scale features in the aircraft trace gas data using passively advected air parcels in coarse resolution velocity fields from global analyses. *Strahan and Mahlman* [1994] offer several suggestions to account for their $k^{-5/3}$ N_2O spectra. They speculate that an underlying k^{-1} tracer spectrum could be steepened by enhanced small-scale diffusion and dissipation induced by cascading enstrophy, gravity wave breaking, or radiative damping.

It is clear that air motions induced by gravity waves can also directly induce variations in trace gas mixing ratios [e.g., *Gary*, 1989 *Danielsen et al.*, 1991; *Chan et al.*, 1993; *Teitelbaum et al.*, 1994; *Reid et al.*, 1994]. The effect of gravity waves on a given trace gas mixing-ratio will depend on the local mixing ratio gradients. For short period gravity waves, vertical gradients will be most important, but for longer-period inertia gravity waves both horizontal and vertical motions will be significant so that horizontal mixing ratio gradients must be considered [e.g., *Teitelbaum et al.*, 1994]. In the studies cited above, gravity wave motions were assumed to act on the large-scale climatological gradients of trace gas mixing ratios to produce variability. This should lead to ozone and N_2O spectra resembling those of potential temperature as argued in section 4.1. However, the average potential temperature spectrum derived here was somewhat steeper (k^{-2} to $k^{-2.5}$) than those observed for ozone and N_2O. Thus an explanation based purely on gravity wave displacements of the background tracer field is not entirely satisfactory either. A more complete theory of trace gas variations due to gravity wave motions may have to include the effect of thin lamina or filaments of trace gases created by quasi-horizontal, enstrophy-cascading 2-D turbulence. Schematically, this would appear as

$$\chi' = \zeta' \frac{\partial}{\partial z} [\overline{\chi}(y,z,t) + \chi^*(x,y,z,t)] \qquad (9)$$

where χ' is the observed trace gas variation, ζ' is a wave-induced vertical displacement, $\overline{\chi}$ is the climatological tracer distribution and χ^* represents tracer variability due to isentropic 2-D turbulent motions (e.g., the filaments simulated by high-resolution parcel advection models). The difference between (9) and earlier studies of gravity-wave-induced variability is in the inclusion of the χ^* term.

The potential effects of these filamentary or laminar structures on gravity-wave-induced variability can be appreciated by examining a typical polar ozone profile as in Figure 15. The profile in Figure 15 was taken on June 30, 1994, at Macquarie Island (159°E, 55°S). Macquarie Island is situated near the climatological edge of the southern winter polar vortex and is thus an ideal location for examining the morphology of vortex erosion. The profile in Figure 15 shows numerous large-amplitude perturbations in ozone mixing ratios with very small vertical scales. Analysis of temperature perturbations for the same balloon flight strongly suggests that these large ozone perturbations are not due to gravity wave motions.

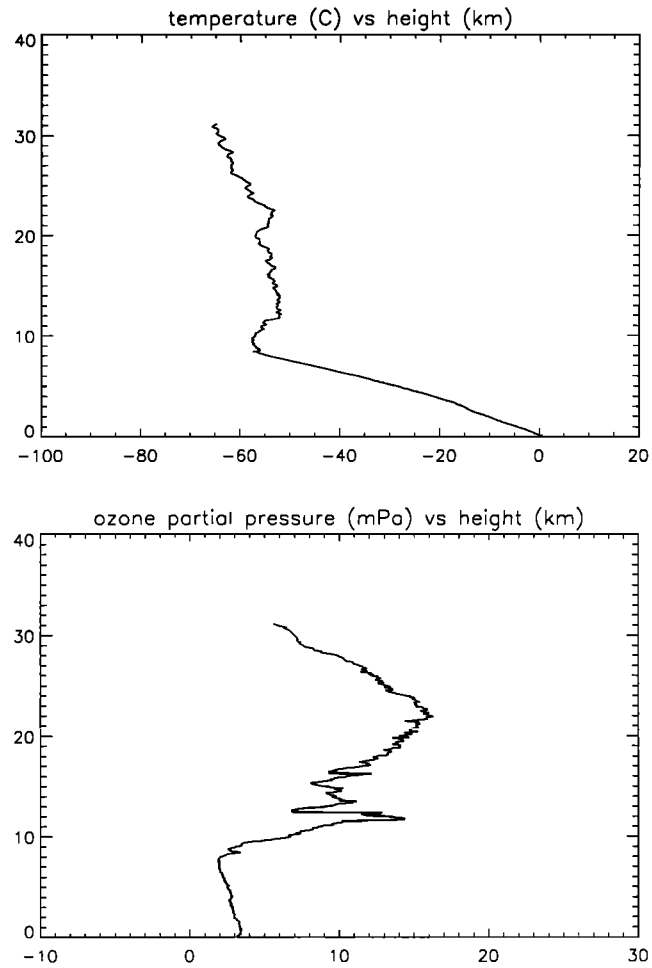

Figure 15. (Top) Temperature and (bottom) ozone partial pressure as a function of altitude over Macquarie Island on June 30, 1994.

A striking feature of the profile in Figure 15 is that the vertical mixing ratio gradients associated with the thin lamina are actually much larger than the mean background gradient. Therefore the total wave-induced tracer variability in (9) may be dominated by the χ^* term. In purely stochastic terms, an important part of the total variablity would then be the product of ζ' a process characterized by a $k^{-2.0}$ or $k^{-2.5}$ spectrum and $\partial_z \chi^*$. Two-dimensional turbulence theory suggests that χ^* is characterized by a k^{-r} spectrum, where r is close to 1 [*Lesieur and Herring*, 1985]. However, the expected horizontal wavenumber spectrum of $\partial_z \chi^*$ cannot be inferred from strictly 2-D theory. Furthermore, the spectral slope of a product of two stochastic sequences may depend on other charcteristics of each sequence, such as intermittency, and is not easily predictable. Thus a prediction of gravity–wave–induced tracer variability appears to require a better understanding of the

3-D morphology of vortex filaments or laminae than is currently available.

The uncertainty in interpreting stratospheric tracer variability also implies that caution should be excercised in interpreting horizontal wavenumber spectra of tracers in other regions of the atmosphere. In particular, horizontal wavenumber spectra derived from lidar measurements of the mesospheric sodium layer [*Kwon et al.*, 1990; *Hostetler and Gardner*, 1994; *Qian et al.*, 1995; *Gardner et al.*, 1995] may include structures analogous to quasi-2-D tracer filaments. Vertical profiles of Na density in so-called sporadic sodium layers [e.g., *Kwon et al.*, 1988] bear similarities to stratospheric ozone profiles such as that in Figure 15. Thus horizontal wavenumber spectra iderived from Na density fluctuations may not be equal to those of the kinetic energy spectra in the mesosphere. Recent analyses by *Qian et al.* [1995] and *Gardner et al.* [1995] report apparent inconsistencies between horizontal wavenumber spectra derived from Na lidar data and those predicted by gravity wave theory using the separable spectra of *Gardner et al.* [1993a,b]. In particular, they find no spectral break to steeper slopes at $k = m_*$ in the horizontal wavenumber spectra of Na density fluctuations. Intsead, the Na spectra of *Qian et al.* [1995] and *Gardner et al.* [1995] look remarkably similar to our ozone and N_2O spectra, exhibiting slopes between -1.3 and -1.8 at horizontal scales smaller than $2\pi/m_*$. It is possible that the observed shape of these Na spectra reflect underlying quasi-horizontal motions rather than the existence of a nonseparable gravity wave spectrum as proposed by *Gardner* [1994].

6. Summary and Conclusions

We have presented horizontal wavenumber spectra for vertical and horizontal velocity, potential temperature, ozone, and N_2O. We used data obtained from a high–altitude ER-2 aircraft during three aircraft campaigns to examine stratospheric chemistry and dynamics; AASE II, SPADE, and ASHOE/MAESA (Table 1). The range of horizontal scales covered by our analysis extends approximately from 400 m to 102 km. The data were taken at altitudes near 20 km during 73 or so flights. The typical duration of each flight was between 6 and 8 hours with a typical aircraft cruise speed of $\approx$400 knots ($\approx$200 m s^{-1}). The total length of the ER-2 flight tracks for the three missions examined exceeds 400,000 km. Although the majority of flight time examined occurred over oceans, a variety of geographical and meteorological conditions was sampled (Figure 1). The results of our spectral analysis using wavelet transforms appeared to be very robust, with both spectral amplitudes as well as spectral slopes between adjacent wavenumbers exhibiting sharply peaked distributions about their respective log-averaged vaules. Therefore we are confident that our results accurately represent "typical" conditions in the midstratosphere (altitudes $\sim$20 km).

Our horizontal and vertical velocity spectra as well as our potential temperature spectra (section 3.1) behave approximately as $k^{-2.5}$ for scales smaller than 6-12 km. At scales longer than 12 km the horizontal velocity and potential temperature spectra approach $k^{-1.5}$ to $k^{-2.0}$ behavior, while the vertical velocity spectrum becomes nearly flat. This range of behaviors cannot currently be explained by a single turbulence theory. The $k^{-2.5}$ behavior at small scales is approximately consistent with theoretical predictions for buoyant subrange turbulence [e.g., *Weinstock*, 1978]. At longer scales the $k^{-1.5}$ to $k^{-2.0}$ behavior is not inconsistent with inverse-cascading 2-D turbulence [e.g. *Gage*, 1979]. We propose an alternative based on spectral transformations of an observationally supported intrinsic frequency-vertical wavenumber gravity wave spectrum shown in Figure 12. This spectrum is transformed to a horizontal wavenumber spectrum for horizontal and vertical velocity using the linear gravity wave dispersion relation. Using this approach, we obtain theoretical spectra that closely match the observed spectra for horizontal and vertical wind. The spectral indices at long and short scales are reproduced as well as the shape of the spectra as they change from the $k^{-2.5}$ behavior at small scales to $k^{-1.6}$ (horizontal velocity) and k^0 (vertical velocity) at the longer scales in our analysis.

The spectra of ozone and N_2O which we derive in section 3.2 behave differently from those of the meteorological quantities. The spectra for these atmospheric tracers exhibit behavior between $k^{-1.5}$ and $k^{-2.0}$ at all scales. This is not entirely consistent with a linear gravity wave interpretation which would predict atmospheric tracer spectra close to those for horizontal velocity and potential temperature. We suggest that this may be due to the presence of strong vertical gradients of mixing ratio produced by enstrophy-cascading 2-D turbulence. The spectrum which would result from the interaction of gravity-wave vertical displacements with such structures in the tracer field is as yet unpredictable.

The analysis presented here is preliminary. The main purpose of the present study was to provide a reliable characterization of typical mesoscale variability in the midstratosphere and to place it in the context of earlier observational and theoretical studies. Although the velocity and potential temperature spectra derived here strongly suggest a gravity wave character for much of the observed variability in the ER-2 data, the spectra for atmospheric tracers such as ozone and N_2O do not appear to conform either to a gravity wave interpretation or to a turbulence interpretation. A complete theory of mesoscale variability in the stratosphere will have to reconcile the wave-like spectra of the meteorological quantities with the anomalous ozone and N_2O spectra. Wavelet transforms are a promising tool for analysis of complex atmospheric data sets such as that collected from the ER-2. We have restricted our attention to power spectra or, in other words, to the second moments of wavelet transforms. This yields information equivalent to that obtained from traditional

Fourier techniques. However, higher order moments of wavelet transforms can be used to quantify other characteristics of data such as intermittency [e.g., *Katul et al.* 1994]. Such analyses of the ER-2 data may shed more light on the dynamical processes producing stratospheric mesoscale variability.

Acknowledgments. This work was partially supported by NASA contract W-18,566. We thank Michael McIntyre and two anonymous reviewers for their helpful comments. We would also like to acknowledge Roger Atkinson, Jim Easson, and Phillip Giese of the Australian Bureau of Meteorology, and Dorothy Gibson-Wilde of the University of Adelaide for making the Macquarie Island ozonesonde data available to us, and for help in using and interpreting the data.

References

Alexander, M. J., and L. Pfister, Gravity wave momentum flux in the lower stratosphere over convection, *Geophys. Res. Lett., 22,* 2029-2032, 1995.

Allen, K. R., and R. I. Joseph, A canonical statistical theory of oceanic internal waves, *J. Fluid Mech., 204,* 185-228, 1989.

Allen, S. J., and R. A. Vincent, Gravity-wave activity in the lower atmosphere: Seasonal and latitudinal variations, *J. Geophys. Res., 100,* 1327-1350, 1995.

Anderson, J. G., and O. B. Toon, Airborne Aircraft Stratospheric Expedition II: An overview, *Geophys. Res. Lett., 20,* 2499-2502, 1993.

Bacmeister, J. T., M. R. Schoeberl, L. R. Lait, P. A. Newman, and B. Gary, ER-2 mountain wave encounter over Antarctica: Evidence for blocking, *Geophys. Res. Lett., 17,* 81-84, 1990a.

Bacmeister, J. T., M. R. Schoeberl, L. R. Lait, P. A. Newman, and B. Gary, Small-scale waves encountered during AASE, *Geophys. Res. Lett., 17,* 349-352, 1990b.

Bacmeister, J. T., P. A. Newman, B. L. Gary, and K. R. Chan, An algorithm for forecasting mountain wave related turbulence in the stratosphere, *Weather and Forecasting, 9,* 241-253, 1994.

Berman, E. A., Meaurements of temperature and downwind spectra in the "buoyant subrange," *J. Atmos. Sci., 33,* 495-498, 1976.

Bolgiano, R., Structure of turbulence in stratified media, *J. Geophys. Res., 67,* 3015-3023, 1962.

Chan, K. R., L. Pfister, T. P. Bui, S. W. Bowen, J. Dean-Day, B. L. Gary, D. W. Fahey, K. K. Kelly, C. R. Webster, and R. D. May, A case study of the mountain lee wave event of January 6, 1992, *Geophys. Res. Lett., 20,* 2551-2554, 1993.

Charney, J. G., Geostrophic turbulence, *J. Atmos. Sci., 28,* 1087-1095, 1971.

Dalaudier, F., and C. Sidi, Evidence and interpretation of a spectral gap in turbulent atmospheric temperature spectra, *J. Atmos. Sci., 44,* 3121-3126, 1987.

Danielsen, E. F., R. S. Hipskind, W. L. Starr, J. F. Vedder, S. E. Gaines, D. Kley, and K. Kelly, Irreversible transport in the stratosphere by internal waves of short vertical wavelength, *J. Geophys. Res., 96,* 17,433-17,452, 1991.

Daubechies, I., Orthonormal bases of compactly supported wavelets, *Commun. Pure Appl. Math., 41,* 909-996, 1988.

Denning, R. F., S. L. Guidero, G. S. Parks, and B. L. Gary, Instrument description of the airborne microwave temperature profiler, *J. Geophys. Res., 94,* 16,757-16,766, 1989.

Eckermann, S. D., Effects of nonstationarity on the spectral analysis of mesoscale motions in the atmosphere, *J. Geophys. Res., 95,* 16,685–16,703, 1990.

Eckermann, S. D., Effect of background winds on the vertical wavenumber spectrum of atmospheric gravity waves, *J. Geophys. Res., 100,* 14,097–14,112, 1995.

Ecklund, W. L., K. S. Gage, G. D. Nastrom, and B. B. Balsley, A preliminary climatology of the atmospheric vertical velocity spectrum observed by clear air radar, *J. Clim. Appl. Meteorol., 25,* 885-892, 1986.

Fritts, D. C., and H.-G. Chou, An investigation of the vertical wavenumber and frequency spectra of gravity wave motions in the lower stratosphere, *J. Atmos. Sci., 44,* 3610-3624, 1987.

Fritts, D. C., and T. E. VanZandt, Effects of Doppler shifting on the frequency spectra of atmospheric gravity waves, *J. Geophys. Res., 92,* 9723-9732, 1987.

Fritts, D. C., and T. E. VanZandt, Spectral estimates of gravity wave energy and momentum fluxes, I: Energy dissipation, acceleration, and constraints, *J. Atmos. Sci., 50,* 3685-3694, 1993.

Fritts, D. C., R. C. Blanchard, and L. Coy, Gravity wave structure between 60 and 90 km inferred from Space Shuttle reentry data, *J. Atmos. Sci., 46,* 423-434, 1989.

Gage, K. S., Evidence for a $k^{-5/3}$ law inertial range in mesoscale two dimensional turbulence, *J. Atmos. Sci., 36,* 1950-1954, 1979.

Gage, K. S., and G. D. Nastrom, On the spectrum of atmospheric velocity fluctuations seen by MST/ST radar and their interpretation, *Radio Sci., 20,* 1339-1347, 1985.

Gage, K. S., and G. D. Nastrom, Spectrum of atmospheric vertical displacements and spectrum of scalar passive additives due to quasi-horizontal atmospheric motions, *J. Geophys. Res., 91,* 13,211-13,216, 1986.

Gage, K. S., and G. D. Nastrom, A simple model for the enhanced frequency spectrum of vertical velocity based on tilting of atmospheric layers by lee waves, *Radio Sci., 25,* 1049-1056, 1990.

Gage, K. S., B. B. Balsley, and R. Garello, Comparisons of horizontal and vertical velocity spectra in the mesosphere, stratosphere, and troposphere: Observations and theory, *Geophys. Res. Lett., 13,* 1125-1128, 1986.

Gardner, C. S., Diffusive filtering theory of gravity wave spectra in the atmosphere, *J. Geophys. Res., 99,* 20,601-20,622, 1994.

Gardner, C. S., and N. F. Gardner, Measurement dis-

tortion in aircraft, space shuttle, and balloon observations at atmospheric density and temperature perturbation spectra, *J. Geophys. Res., 98,* 1023-1033, 1993.

Gardner, C. S., C. A. Hostetler, and S. J. Franke, Gravity wave models for the horizontal wave number spectra of atmospheric velocity and density perturbations, *J. Geophys. Res., 98,* 1035-1049, 1993a.

Gardner, C. S., C. A. Hostetler, and S. Lintelman, Influence of the mean wind field on the separability of atmospheric perturbation spectra, *J. Geophys. Res., 98,* 8859-8872, 1993b.

Gardner, C. S., J. Qian, M. R. Coble, G. C. Papen, and G. R. Swenson, High resolution horizontal wave number spectra of mesospheric wave perturbations observed during the 21 October triangular flight of ALOHA-93, *Geophys. Res. Lett., 22,* 2869-2872, 1995.

Gary, B. L., Observational results using the microwave temperature profiler during the Airborne Antarctic Ozone Experiment, *J. Geophys. Res., 94,* 11,223-11,231, 1989.

Hines, C. O., The saturation of gravity waves in the middle atmosphere, II: Development of Doppler-spread theory, *J. Atmos. Sci., 48,* 1360-1379, 1991.

Hocking, W. K., Measurements of turbulent energy dissipation rates in the middle atmosphere by radar techniques: A review, *Radio Sci., 20,* 1403-1422, 1985.

Hostetler, C. A., and C. S. Gardner, Observations of horizontal and vertical wave number spectra of gravity wave motions in the stratosphere and mesosphere over the mid-Pacific, *J. Geophys. Res., 99,* 1283-1302, 1994.

Katul, G. G., M. B. Parlange, and C. R. Chu, Intermittency, local isotropy, and non-gaussian statistics in atmospheric surface layer turbulence, *Phys. Fluids, 6,* 2480-2492, 1994.

Koprov, B. M., Spectra of turbulent fluctuations of vertical wind-velocity component in boundary layer with developed convection. *Izv. Akad. Nauk. SSSR Fiz. Atmos. Okeana, 1*(11), 1151-1160, 1965.

Kraichnan, R., Inertial ranges in two-dimensional turbulence, *Phys. Fluids, 10,* 1417-1423, 1967.

Kwon, K. H., D. C. Senft, and C. S. Gardner, Lidar observations of sporadic sodium layers at Mauna Kea Observatory, Hawaii, *J. Geophys. Res.*, 93, 14,199-14,208, 1988.

Kwon, K. H., D. C. Senft, and C. S. Gardner, Airborne sodium lidar observations of horizontal and vertical wave number spectra of mesopause density and wind perturbations, *J. Geophys. Res.*, 95, 13,723-13,736, 1990.

Lait, L. R., et al., Reconstruction of O_3 and N_2O fields from ER-2, DC-8, balloon observations, *Geophys. Res. Lett., 17,* 521-524, 1990.

Lesieur, M., and J. Herring, Diffusion of a passive scalar in two-dimensional turbulence, *J. Fluid. Mech., 161,* 77-95, 1985.

Lilly, D. K., Stratified turbulence and the mesoscale variability of the atmosphere, *J. Atmos. Sci., 40,* 749-761, 1983.

Lilly, D. K., and P. F. Lester, Waves and turbulence in the stratosphere, *J. Atmos. Sci., 31,* 800-812, 1974.

Lilly, D. K., and E. L. Petersen, Aircraft measurements of atmospheric kinetic energy spectra, *Tellus, 35A,* 379-382, 1983.

Lin, J.-T., and Y.-H. Pao, Wakes in stratified fluids, *Ann. Rev. Fluid Mech., 11,* 317-338, 1979.

Loewenstein, M., J.R. Podolske, K.R. Chan, and S.E. Strahan, Nitrous oxide as a dynamical tracer in the 1987 Airborne Antarctic Ozone Experiment, *J. Geophys. Res., 94,* 11,589-11,598, 1989.

Lumley, J. L., The spectrum of nearly inertial turbulence in a stably stratified fluid, *J. Atmos. Sci., 21,* 99-102, 1964.

Mallat, S. G., A theory for multiresolution signal decomposition: The wavelet representation, *IEEE Trans. Pattern Anal. Machine Intell., 11,* 674-693, 1989.

McWilliams, J. C., The emergence of isolated coherent vortices in turbulent flow, *J. Fluid Mech., 146,* 21-43, 1984.

Murphy, D., Time offsets and power spectra of the ER-2 data set from the 1987 Airborne Antarctic Ozone Experiment, *J. Geophys. Res., 94,* 16,737-16,748, 1989.

Myrup, L. O., Atmospheric measurements of the buoyant subrange of turbulence, *J. Atmos. Sci., 25,* 1160-1164, 1968.

Nastrom, G. D., and D. C. Fritts, Sources of mesoscale variability of gravity waves, I: Topographic excitation, *J. Atmos. Sci., 49,* 101-110, 1992.

Nastrom, G. D., and K. S. Gage, A climatology of atmospheric wavenumber spectra observed by commercial aircraft, *J. Atmos. Sci., 42,* 950-960, 1985.

Nastrom, G. D., K. S. Gage, and W. H. Jasperson, Atmospheric kinetic energy spectrum, $10^0 - 10^4$ km, *Nature, 310,* 36-38, 1984.

Nastrom, G. D., W. H. Jasperson, and K. S. Gage, Horizontal spectra of atmospheric tracers measured during the Global Atmospheric Sampling Program, *J. Geophys. Res., 91,* 13,201-13,209, 1986.

Nastrom, G. D., D. C. Fritts, and K. S. Gage, An investigation of terrain effects on the mesoscale spectrum of atmospheric motions, *J. Atmos. Sci., 44,* 3087-3096, 1987.

Newman, P. A., L. R. Lait, M. R. Schoeberl, E. R. Nash, K. Kelly, D. Fahey, R. M. Nagatani, D. W. Toohey, L. M. Avallone, and J. G. Anderson, Stratospheric meteorological conditions in the Arctic polar vortex, 1991-1992, *Science, 261,* 1143-1146, 1993.

Pfister, L., K. R. Chan, T. P. Bui, S. W. Bowen, M. Legg, B. L. Gary, K. K. Kelly, M. H. Proffitt, and W. Starr, Gravity waves generated by a tropical cyclone during the STEP tropical field program: A case study, *J. Geophys. Res., 98,* 8611-8638, 1993.

Pierce, R. B., W.J. Grose, J. M. Russell, A. F. Tuck, R. Swinbank, and A. O'Neill, Spring dehydration in the stratospheric vortex observed by HALOE, *J. Atmos. Sci., 51,* 2931-2941, 1994.

Plumb, R. A., D. W. Waugh, R. J. Atkinson, P. A. Newman, L. R. Lait, M. R. Schoeberl, E. V. Browell, A. J. Simmons, and M. Loewenstein, Intrusions into the lower stratospheric vortex during the winter of 1991-1992, *J. Geophys. Res., 99,* 1089-1105, 1994.

Podolske, J. R., M. Loewenstein, S. E. Strahan, and K. R. Chan, Stratospheric nitrous oxide distribution in the southern hemisphere, *J. Geophys. Res., 94,* 16,767-16,772, 1989.

Powell, D. C., and C. E. Elderkin, An investigation of the application of Taylor's hypothesis to atmospheric boundary layer turbulence, *J. Atmos. Sci., 31,* 990-1002, 1974.

Press, W. H., S. A. Teukolsky, W. T. Vetterling, and B. P. Flannery, *Numerical Recipes in FORTRAN,* 2nd ed., 963 pp., Cambrige Univ. Press, New York, 1992.

Proffitt, M. H., et al., In situ ozone measurements within the 1987 ozone hole from a high-altitude ER-2 aircraft, *J. Geophys. Res., 94,* 16,547-16,556, 1989.

Qian, J., Y. Y. Gu, G. C. Papen, C. S. Gardner, and P. J. Espy, Horizontal wave number spectra of density and temperature perturbations in the mesosphere measured during the 4 August flight of ANLC-93, *Geophys. Res. Lett., 22,* 2865-2868, 1995.

Reid, S. J., G Vaughan, N. J. Mitchell, I. T. Pritchard, H. J. Smit, T. S. Jorgensen, C. Varostos, and H. de Becker, Distribution of ozone laminae and the possible influence of inertia-gravity waves, *Geophys. Res. Lett., 21,* 1479-1482, 1994.

Russell, P. B., L. Pfister, and H. B. Selkirk, The tropical experiment of the Stratosphere-Troposphere Exchange Project (STEP): Science objectives, operations, and summary findings, *J. Geophys. Res., 98,* 8563-8590, 1993.

Scheffler, A. O., and C. H. Liu, The effects of Doppler shift on gravity wave spectra observed by MST radar, *J. Atmos. Terr. Phys., 48,* 1225-1231, 1986.

Schoeberl, M. R., S. D. Doiron, L. R. Lait, P. A. Newman, and A. J. Krueger, A simulation of the Cerro Hudson SO_2 cloud, *J. Geophys. Res., 98,* 2949-2957, 1993.

Schoeberl, M. R., A. R. Douglass, R. S. Stolarski, P. A. Newman, L. R. Lait, D. W. Toohey, L. M. Avallone, J. G. Anderson, W. Brune, D. W. Fahey, and K. Kelly, The evolution of ClO and NO along air parcel trajectories, *Geophys. Res. Lett., 20,* 2511-2514, 1993.

Scott, S. G., T. P. Bui, K.R. Chan, S.W. Bowen, The meteorological measurement system on the NASA ER-2 aircraft., *J. Atmos. Ocean. Tech., 7,* 525-540, 1990.

Shur, G. N., Experimental investigations of the energy spectrum of atmospheric turbulence. *Tr. Tsentra. Aerolog. Observ., 43* 79-90, 1962. (Engl. Transl. *AID Rep. T-63-55,* Aerospace Inf., Library of Congress, Washington, D. C.)

Shur, G. N., Aircraft investigations of clear air turbulence in the troposphere and stratosphere, in *Proceedings of the All-Union Conferences on Questions of Meteorological Support for Supersonic Aviation* pp.141-149 [in Russian], Izd. LGMI, Moscow, 1971.

Sidi, C., and F. Dalaudier, Temperature and heat flux spectra in the turbulent buoyancy subrange, *Pure Appl. Geophys., 130,* 547-569, 1989.

Smith, S. A., D. C. Fritts, and T. E. VanZandt, Evidence of a saturated spectrum of atmospheric gravity waves, *J. Atmos. Sci., 44,* 1404-1410, 1987.

Strahan, S., and J. D. Mahlman, Evaluation of the SKYHI general circulation model using aircraft N_2O measurements, 2. Tracer variability and diabatic meridional circulation, *J. Geophys. Res., 99,* 10,319-10,332, 1994.

Teitelbaum, H., J. Ovarlez, H. Kelder, and F. Lott, Some observations of gravity wave induced structure in ozone and water vapour during EASOE, *Geophys. Res. Lett., 21,* 1483-1486, 1994.

Tennekes, H., and J. L. Lumley, *A first Course in Turbulence,* 300 pp., MIT Press, Cambridge, Mass., 1972.

Tjemkes, S. A., and M. Visser, Horizontal variability of temperature, specific humidity, and cloud liquid water as derived from spaceborne observations, *J. Geophys. Res., 99,* 23,089-23,105, 1994.

Tsuda, T., T. E. VanZandt, M. Mizumoto, S. Kato, and S. Fukao, Spectral analysis of temperature and Brunt-Väisälä frequency fluctuations observed by radiosondes, *J. Geophys. Res., 96,* 17,265-17,278, 1991.

Tuck, A. F., R. T. Watson, E. P. Condon, J. J. Margitan, and O. B. Toon, The planning and execution of ER-2 and DC-8 aircraft flights over Antarctica, August and September 1987, *J. Geophys. Res., 94,* 11,181-11,222, 1989.

Turco, R., R. A. Plumb, and E. P. Condon, The Airborne Aircraft Stratospheric Expedition: Prologue, *Geophys. Res. Lett., 17,* 313-316, 1990.

VanZandt, T. E., G. D. Nastrom, and J. L. Green, Frequency spectra of vertical velocity from Flatland VHF radar data, *J. Geophys. Res., 96,* 2845-2855, 1991.

Vincent, R. A., and S. D. Eckermann, VHF radar observations of mesoscale motions in the atmosphere: Evidence for gravity wave Doppler shifting, *Radio Sci., 25,* 1019–1037, 1990.

Vinnichenko, N. K., N. Z. Pinus, and G. N. Shur, Some results of experimental investigations of turbulence in the troposphere, in *International Colloquium on the Fine Scale Structure of the Atmosphere and its Relation to Radio-Wave Propagation* (in Russian), Nauka, Moscow, 1965.

Vinnichenko, N. K., N. Z. Pinus, S. M. Shmeter and G. N. Shur, *Turbulence in the Free Atmosphere,* 2nd ed., 310 pp., Plenum, New York, 1980.

Waugh, D. W., and R. A. Plumb, Contour advection with surgery: A technique for investigating fine scale structure in tracer transport, *J. Atmos. Sci., 51,* 530-540, 1994.

Waugh, D. W., et al., Transport out of the lower stratospheric vortex by Rossby wave breaking, *J. Geophys. Res., 99,* 1089-1105, 1994.

Weinstock, J. D., On the theory of turbulence in the buoyancy subrange of stably stratified flows, *J. Atmos. Sci., 35,* 634-649, 1978.

Weinstock, J. D., Theoretical gravity wave spectrum: Strong and weak wave interactions, *Radio Sci., 20,* 1295-1300, 1985a.

Weinstock, J. D., On the theory of temperature spectra in a stably stratified fluid, *J. Phys. Oceanogr., 15,* 475–477, 1985b.

Weinstock, J. D., Saturated and unsaturated spectra of gravity waves, and scale dependent diffusion, *J. Atmos. Sci., 47,* 2211-2225, 1990.

Weinstock, J. D., Vertical diffusivity and overturning length in stably stratified turbulence, *J. Geophys. Res., 97,* 12,653-12,658, 1992.

Wyngaard, J. C., and S. F. Clifford, Taylor's hypothesis and high-frequency turbulence spectra, *J. Atmos. Sci., 34,* 922-929, 1977.

Yamada, M., and K. Ohkitani, Orthonormal wavelet analysis of turbulence, *Fluid. Dyn. Res., 8,* 101-115, 1991.

Yuan, L., and K. P. Hamilton, Equilibrium dynamics in a forced dissipative f-plane shallow water system, *J. Fluid Mech., 280,* 369-394, 1994.

Zhu, X., A new theory of the saturated gravity wave spectrum for the middle atmosphere, *J. Atmos. Sci., 51,* 3615-3626, 1994.

Julio T. Bacmeister, Naval Research Laboratory, Washington D.C., 20375 (e-mail: julio@ismap5.nrl.navy.mil)

K. Roland Chan and Max Loewenstein, NASA Ames Research Center, Moffet Field, CA, 94035

Stephen D. Eckermann,, Computational Physics, Inc., Fairfax, VA, 22031 (e-mail: eckerman@ismap4.nrl.navy.mil)

Bruce L. Gary, NASA Jet Propulsion Laboratory, Pasadena, CA, 91109

Paul A. Newman and Leslie Lait, NASA Goddard Space Flight Center, Greenbelt, MD, 20771

Michael H. Proffitt, NOAA Aeronomy Laboratory and CIRES University of Colorado, Boulder, CO 80303

(Received May 18, 1995; revised November 10, 1995; accepted November 10, 1995.)